

Isovector $E2$ matrix elements from electromagnetic transitions in the s - d shell: Experiment and shell-model calculations

B. A. Brown*

*Nuclear Physics Laboratory, Oxford University, Oxford, England OX1 3RH
and Cyclotron Laboratory, Michigan State University, East Lansing, Michigan 48824*

B. H. Wildenthal and W. Chung

Cyclotron Laboratory, Michigan State University, East Lansing, Michigan 48824

S. E. Massen*

*Nuclear Physics Laboratory, Oxford University, Oxford, England OX1 3RH
and Department of Theoretical Physics, University of Thessaloniki, Thessaloniki, Greece*

M. Bernas

Institut de Physique Nucléaire, Orsay, France 91406

A. M. Bernstein and R. Miskimen

*Physics Department and Laboratory for Nuclear Science, Massachusetts Institute of Technology,
Cambridge, Massachusetts 02139*

V. R. Brown and V. A. Madsen[†]

Lawrence Livermore National Laboratory, Livermore, California 94550

(Received 25 June 1982)

All available $B(E2)$ values in the mass region $8 \leq Z$, $N \leq 20$ relevant to the isovector electric quadrupole operator are compared to the theoretical $B(E2)$ values based on Chung-Wildenthal $0d_{5/2}-1s_{1/2}-0d_{3/2}$ shell-model wave functions with harmonic oscillator radial wave functions, and some selected cases are compared with local and energy dependent Woods-Saxon potential wave functions. The empirical effective charges deduced from these comparisons are insensitive to differences in mass, state, and dominant single-nucleon orbit. The value for the effective charge parameter $e_p - e_n$ extracted in the harmonic oscillator approximation is consistent with $1.0e$. The values extracted with local and energy-dependent Woods-Saxon potentials, which are more meaningfully related to the underlying structure of the isovector polarizability, are consistent with $0.7e$ and $0.6e$, respectively. Some inadequacies in the experimental data and theoretical models are discussed and improvements are suggested.

NUCLEAR STRUCTURE $17 \leq A \leq 39$ nuclei: comparison of experimental $E2$ isovector matrix elements with shell-model predictions; extraction of the isovector effective charge; full basis $0d_{5/2}-1s_{1/2}-0d_{3/2}$ shell-model wave functions; Chung-Wildenthal Hamiltonians.

I. INTRODUCTION

We are concerned in this paper with the isovector (IV) component of electric quadrupole ($E2$) transitions between nuclear states. We extract experimental values for $E2_{IV}$ matrix elements from radiative transition data in the region $8 \leq N$, $Z \leq 20$ and compare these results with the predictions of the shell-model wave functions (complete $d_{5/2}-s_{1/2}-d_{3/2}$ basis

space) of Chung and Wildenthal.¹ Our first aim is to establish the extent to which the conventional shell-model approximations can account for these data. The key approximations in this context are the restriction to one-body operators (the "impulse approximation") and the factorization of matrix elements into an explicitly state-dependent, "intra-model-space" term (the shell-model transition densities) and an approximately state-independent,

“extra-model-space” term (the “effective charges” in the case of electric transitions). A subsidiary aspect of these approximations which is critically examined in the present work is that of the radial dependence of the single-particle wave functions. Our second aim, which can be pursued to the degree that there appears to be a meaningful relationship between theoretical and experimental matrix elements, is to deduce the empirically optimum value of the $E2_{IV}$ effective charge.

The approximate charge independence of the strong interaction leads to the approximate conservation of isospin for nuclear states. In many shell-model calculations, including those of Chung and Wildenthal, this approximate conservation of isospin is introduced *ab initio* into the model via a precisely charge-independent Hamiltonian and the resulting wave functions are labeled by the total isospin quantum number on an equivalent footing with the total angular momentum quantum number.

The consequence of this is that in terms of configuration mixing of shell-model orbitals the same many-body wave function $|v, J, T, A\rangle$ is manifested in each of the $(2T+1)$ members of an isobaric spin multiplet, each member being labeled by $T_Z = (Z-N)/2$. The only changes in the wave function as T_Z changes is the apportionment between neutrons and protons of the nucleons which constitute the A -particle wave function. Since electric multipole transitions involve only the proton components of the wave functions of the initial and final states, the $B(E\lambda)$ value for a transition

$$|v_i J_i T_i A\rangle \rightarrow |v_f J_f T_f A\rangle$$

will be different for each nucleus A, T_Z in the isobaric multiplet. Under the assumption of good isospin there are simple relationships between the isoscalar and isovector, or equivalently, the proton and neutron, components of a transition in a particular A, T_Z and the (different) proton and neutron components of the analogous transition in another nucleus of that isospin multiplet.² In particular, for isospin doublets and triplets, $T_Z = \pm \frac{1}{2}$ and ± 1 , the proton component in the $T_Z = +T$ nucleus is equal to the neutron component in the $T_Z = -T$ nucleus.³

We have exploited this symmetry in the present work by comparing proton transition matrix elements M_p from $B(E2)$ values for pairs of transitions

$$\{ |v_i J_i T_i\rangle \rightarrow |v_f J_f T_f\rangle \}_{T_Z = \pm T}.$$

This comparison of M_p in the two different nuclei

yields the relative proton and neutron matrix elements M_p and M_n in either of the two nuclei separately. Equivalently, the sum and difference of these matrix elements yields the isoscalar and isovector strengths for the transition. We note that not all nuclear transitions have both isovector and isoscalar components. Transitions of $T_i=0 \rightarrow T_f=0$ are purely isoscalar, i.e., the proton and neutron matrix elements are equal, and transitions for which $T_i \rightarrow (T_f = T_i \pm 1)$ are purely isovector, i.e., the neutron and proton matrix elements, are equal in magnitude but opposite in sign.

It appears from experimental observation that most strong electric quadrupole ($\Delta J^\pi = 2^+$) transitions are dominated by their isoscalar component. This feature is consistent with our understanding of the short-range, attractive nature of the nucleon-nucleon force. Isoscalar dominance also emerges from explicit model calculations such as those of Chung and Wildenthal.^{1,2} As a consequence of this typical isoscalar dominance and of the inescapable residues of experimental (and nuclear model) errors, our knowledge of the isovector aspects of $E2$ phenomena is quite limited. Hence it follows that our knowledge of the differences between the neutron and proton components of transitions in a given nucleus is equivalently limited. From the standpoint of better characterizing experimental nuclear transitions and to better test nuclear wave functions, it is desirable to know the relative strengths of their neutron and proton (or isoscalar and isovector) matrix elements individually.

The experimental data on electromagnetic transitions we consider here provide the classical avenue to study of the subject of isovector strength or relative neutron/proton transition strengths. Analysis of these data is facilitated by the fact that the electromagnetic field operator is the best understood probe of the nucleus. However, as we shall discuss, the conclusions which can be drawn from the data depend significantly upon the degree to which isospin nonconserving features, specifically differences in radial wave functions of the protons and neutrons, affect the empirically extracted values. Moreover, in practical terms, the errors in the $B(E2)$ values of decays in proton-rich nuclei are sometimes so large as to vitiate the extraction of the isovector strength via comparison to the neutron-rich values.

II. THEORETICAL ASPECTS

A. Definition of the operators

The λ -multipole transition operator for the protons in a nucleus is defined by

$$\begin{aligned}
O_p^\lambda &\equiv \sum_i^Z r_i^\lambda Y_\mu^\lambda(\Omega_i) \\
&= \sum_i^A \left[\frac{1+\tau_{zi}}{2} \right] r_i^\lambda Y_\mu^\lambda(\Omega_i) \\
&= \frac{1}{2} \sum_i^A r_i^\lambda Y_\mu^\lambda(\Omega_i) + \frac{1}{2} \sum_i^A \tau_{zi} r_i^\lambda Y_\mu^\lambda(\Omega_i) \\
&\equiv 0_{\Delta T=0}^\lambda + 0_{\Delta T=1}^\lambda .
\end{aligned} \tag{1}$$

We use the convention $\tau_z |p\rangle = +|p\rangle$ and $\tau_z |n\rangle = -|n\rangle$. The analogous λ multipole operator for neutrons is correspondingly

$$O_n^\lambda = O_0^\lambda - O_1^\lambda . \tag{2}$$

The complete matrix element $M_{p/n}$ for a transition between initial (i) and final (f) nuclear states $|\nu_i J_i T_i T_Z A\rangle$ and $|\nu_f J_f T_f T_Z A\rangle$ is assumed to be

$$M_{p/n}(T_Z) = \langle \nu_f J_f T_f T_Z A || 0_{p/n}^\lambda || \nu_i J_i T_i T_Z A \rangle , \tag{3}$$

$$\begin{aligned}
M_{p/n}(T_Z) &= \frac{(-1)^{T_f - T_Z}}{2} \left[\begin{array}{cc} T_f & 0 & T_i \\ -T_Z & 0 & T_Z \end{array} \right] \langle \nu_f J_f T_f A || | 0_0^\lambda || | \nu_i J_i T_i A \rangle \\
&\quad + / - \left[\begin{array}{cc} T_f & 1 & T_i \\ -T_Z & 0 & T_Z \end{array} \right] \langle \nu_f J_f T_f A || | 0_1^\lambda || | \nu_i J_i T_i A \rangle .
\end{aligned} \tag{6}$$

It follows that for $T_i = T_f = T$

$$\begin{aligned}
M_{p/n}(T_Z) &= (2T+1)^{-1/2} \langle \nu_f J_f T_f A || | 0_0^\lambda || | \nu_i J_i T_i A \rangle \\
&\quad + / - T_Z [(2T+1)(T+1)(T)]^{-1/2} \langle \nu_f J_f T_f A || | 0_1^\lambda || | \nu_i J_i T_i A \rangle \\
&\equiv M_0 + / - T_Z M_1 ,
\end{aligned} \tag{7a}$$

and that for transitions characterized by $|T_i - T_f| = 1$ and for $T_i = T_f = 0$, only the isovector and isoscalar terms of Eq. (6) contribute, respectively;

$$M_1 = [(2T+1)(T+1)(T)]^{-1/2} \langle \nu_f J_f T_f A || | 0_1^\lambda || | \nu_i J_i T_i A \rangle , \tag{7b}$$

$$M_0 = (2T+1)^{-1/2} \langle \nu_f J_f T_f A || | 0_0^\lambda || | \nu_i J_i T_i A \rangle . \tag{7c}$$

The relationship of Eq. (7) establishes the equality, pointed out in Ref. 3, which exists between the neutron transition matrix element $M_n(T_Z = -T)$ in the neutron-rich nucleus and the proton transition matrix element, $M_p(T_Z = +T)$, for the same pair of states in the isobaric analog proton-rich nucleus:

$$M_n(T_Z = -T) = M_p(T_Z = +T) . \tag{8}$$

It is this equality which provides a connection between the electromagnetic decay probabilities to the

where J is the total angular momentum, T the isospin, and $T_Z = \frac{1}{2}(Z - N)$; the indices "v" supply the additional labels needed to uniquely specify the states. The reduced matrix elements are defined by

$$\begin{aligned}
\langle JM | Y_\mu^\lambda | J'M' \rangle &= (-1)^{J-M} \begin{bmatrix} J & \lambda & J' \\ -M & \mu & M' \end{bmatrix} \\
&\quad \times \langle J || Y^\lambda || J' \rangle .
\end{aligned} \tag{4}$$

In this convention the electromagnetic transition probability is given as

$$B(E\lambda, i \rightarrow f) = (2J_i + 1)^{-1} M_p^2 e^2 . \tag{5}$$

B. Isospin dependence of the matrix elements

In terms of matrix elements reduced with respect to both J and T ("triple-barred" matrix elements)

ground states of nuclear isobaric multiplets and the reduced strengths for inelastic excitation of the (stable) neutron-rich members of these multiplets by hadrons which interact with both protons and neutrons.

Our present interest is focused on isovector matrix elements M_1 which can be extracted from $E2$ electromagnetic decay data. These matrix elements can be obtained experimentally either directly from the electromagnetic matrix elements M_p for isospin-changing transitions ($\Delta T = 1$) or from the

differences between the values of M_p of a transition

$$|v_i J_i T_i\rangle \rightarrow |v_f J_f T_f\rangle$$

as this transition is manifested in the various T_Z members on an isobaric nuclear multiplet. For $T \neq 0$, we can rewrite Eq. (7) as

$$M_1 = [M_p(T_Z) - M_p(T_Z - \Delta T_Z)] / \Delta T_Z. \quad (9)$$

Since only M_p^2 is extracted from experimental decay data the phase relation is not known and we will define a quantity ΔM_p as

$$\Delta M_p = \{ |M_p(T_Z)| \pm |M_p(T_Z - \Delta T_Z)| \} / \Delta T_Z, \quad (10)$$

where the sign is to be determined theoretically so that $M_1 = \pm \Delta M_p$. Usually,

$$|M_0| > |T_Z M_1|,$$

and hence, M_1 is obtained by taking the difference rather than sum in Eq. (10). The sign can also be determined experimentally via Eq. (8) by inelastic scattering of hadrons which are sensitive to both $M_n(T_Z = -T)$ and $M_p(T_Z = -T)$.

Most of the available data related to these differences come from mirror nuclei with $T_Z = \pm \frac{1}{2}$ and $T_Z = \pm 1$. A few $T = 1 \rightarrow T = 1$ transitions strengths have been measured in $T_Z = 0$ nuclei. The plots of $M_p(T_Z)$ vs T_Z for the three members of these $T = 1$ triplets should be linear in T_Z according to Eq. (7). A few electromagnetic $E2$ transitions with $|T_i - T_f| = 1$ have been measured and these pro-

vide direct information on the isovector matrix elements.

C. The shell-model plus core-polarization approximation

Our theoretical estimates of the "total" matrix elements $M_{p/n}$ are obtained from "model space" matrix elements $A_{p/n}$ calculated from shell-model wave functions. The basis space assumed for the shell-model wave function of a state in nucleus A is the complete set of $0d_{5/2}$, $1s_{1/2}$, and $0d_{3/2}$ configurations for $n = A - 16$ nucleons, abbreviated $(sd)^n$. The wave functions $|(sd)^n, vJT\rangle$ result from diagonalizing the Chung-Wildenthal "particle" and "hole" Hamiltonians for the regions $A = 17 - 28$ and $A = 28 - 39$, respectively, in the $(sd)^n$ space.

The model-space transition matrix elements $A_{p/n}(T_Z)$ are calculated from these wave functions according to

$$A_{p/n}(T_Z) = \langle (sd)^n v_f J_f T_f T_Z | |0_{p/n}^\lambda | | (sd)^n v_i J_i T_i T_Z \rangle \\ = \sum_{jj'}^{(sd)} \text{SPME}[0_{p/n}^\lambda(jj')] D_{\lambda,p/n}^{n,i,f,T_Z}(jj'), \quad (11)$$

where the single particle matrix elements (SPME) of the operator $0_{p/n}^\lambda$ between the single nucleon states of the model space ρ_j and $\rho_{j'}$ are given by

$$\text{SPME}[0_{p/n}^\lambda(jj')] \equiv \langle \rho_j | |0_{p/n}^\lambda | | \rho_{j'} \rangle, \quad (12)$$

and the one-body density matrix elements D between the n -body shell-model wave functions are given by

$$D_{\lambda,p/n}^{n,i,f,T_Z} \equiv (2\lambda + 1)^{-1/2} \langle (sd)^n v_f J_f T_f T_Z | | (a_j^\dagger \times \tilde{a}_{j'})_{p/n}^\lambda | | (sd)^n v_i J_i T_i T_Z \rangle. \quad (13)$$

The p/n representation of the matrix elements A is related to the $\Delta T = 0$ and 1 isospin coupled representation by

$$D_{\lambda,p/n}^{T_Z} = \frac{(-1)^{T_f - T_Z}}{2} \left\{ \sqrt{2} \begin{bmatrix} T_f & 0 & T_i \\ -T_Z & 0 & T_Z \end{bmatrix} D_{\lambda,\Delta T=0} + / - \sqrt{6} \begin{bmatrix} T_f & 1 & T_i \\ -T_Z & 0 & T_Z \end{bmatrix} D_{\lambda,\Delta T=1} \right\}, \quad (14)$$

where

$$D_{\lambda,\Delta T} = [(2\lambda + 1)(2\Delta T + 1)]^{-1/2} \langle (sd)^n v_f J_f T_f | | (a_j^\dagger \times \tilde{a}_{j'})_{\Delta T}^\lambda | | (sd)^n v_i J_i T_i \rangle,$$

and similarly for the single particle matrix elements

$$\text{SPME}(0_{p/n}^\lambda) = \frac{1}{\sqrt{2}} \langle \rho_j | | 0_{\Delta T=0}^\lambda | | \rho_{j'} \rangle + / - \frac{1}{\sqrt{6}} \langle \rho_j | | 0_{\Delta T=1}^\lambda | | \rho_{j'} \rangle. \quad (15)$$

The one-body densities $D_{\lambda,p/n}$ contain all of the information about the transition in question which is embedded in the configuration-mixing amplitudes of the two $(sd)^n$ shell-model wave functions. The single-particle matrix elements $\text{SPME}(0_{p/n}^\lambda)$ incor-

porate our assumptions about the transition operators and about the radial dependences of the single-nucleon wave function ρ_j . The principal body of the theoretical results we present and discuss in this paper are obtained under the assumption of har-

monic oscillator radial dependence for the single-nucleon wave functions. For each A value, the oscillator length parameter is chosen to reproduce the root mean square (rms) charge radius of the stable ground state. The details of the calculations of the length parameter and the consequent “ b ” values are given in Ref. 4. The consequences of choosing other forms for the single-nucleon radial dependence are discussed in Sec. V.

In terms of these model-space matrix elements $A_{p/n}$, the total matrix elements $M_{p/n}$ are assumed to be given by

$$\begin{aligned} M_p &= A_p(1 + \delta_{pp}) + A_n \delta_{pn} , \\ M_n &= A_n(1 + \delta_{nn}) + A_p \delta_{np} . \end{aligned} \quad (16)$$

Thus, it is assumed that the total matrix elements $M_{p/n}$, which in principle incorporate excitation of all Z/N protons/neutrons in the nucleus over indefinitely many shell-model orbits can be expressed as the model-space matrix elements $A_{p/n}$ modified by the addition of two other terms, themselves simply proportional to the same model-space elements A_p and A_n .

This can be termed the “effective charge” core-polarization model. The quantity δ_{cv} denotes the renormalization due to the polarization of the core nucleons (c) by the valence model-space nucleons (v). Since the core in the present shell-model has equal numbers of neutrons and protons it is a good approximation to equate $\delta_{pp} = \delta_{nn}$ and $\delta_{pn} = \delta_{np}$. The “effective charges” for the $E\lambda$ electromagnetic transitions are then $e_p = (1 + \delta_{pp})e$ and $e_n = \delta_{pn}e$ and in units of e ,

$$M_p = [A_p e_p + A_n e_n] , \quad (17)$$

$$M_n = [A_n e_p + A_p e_n] ,$$

or

$$M_1 = A_1(e_p - e_n) , \quad (18)$$

where the isovector model-space matrix element A_1 has the same relationship to A_p and A_n as M_1 does to M_p and M_n . Thus, our theoretical representation of the total transition matrix element for an isovector electric-quadrupole transition is the product of a term which comes from the model-space $(sd)^n$ wave functions and a term, $(e_p - e_n)$, which depends upon the effective isovector polarization for this model space. A y - x plot of experimental values of M_1 versus their theoretical model-space analogs A_1 should, under these assumptions, thus yield a straight line through the origin which has a slope given by $(e_p - e_n)$.

III. EXPERIMENTAL DATA AND COMPARISON WITH THEORY

A. Compiled data

The primary source of our experimental information is the most recent compilation by Endt⁵ of the electromagnetic strengths in nuclei with $A = 6-44$. For data on some transitions which are not included by Endt we use the adopted average values in the $A = 21-44$ compilation of Endt and van der Leun.⁶ In either case we start from the adopted average values for the initial state mean lifetime τ , the initial and final state energies E_i and E_f , and the branching ratio BR and mixing ratio $\delta(E2/M1)$ for the transition to the final state and calculate the $B(E2)$ value,

$$B(E2) = \frac{816 e^2 \text{fm}^4}{|E_i - E_f|^5} \frac{\text{BR}}{\tau} \frac{\delta^2}{1 + \delta^2} , \quad (19)$$

where E is in units of MeV and τ is in units of ps. The $B(E2)$ in units of $e^2 \text{fm}^4$ can be converted to Weisskopf units by dividing by $0.0594 A^{4/3} e^2 \text{fm}^4$. For $A = 17, 28,$ and 39 the Weisskopf units are 2.60, 5.05, and $7.86 e^2 \text{fm}^4$, respectively. In Table I we list the experimental information together with the experimental values for the matrix elements M_p given by

$$M_p = [(2J_i + 1)B(E2)]^{1/2} / e$$

together with the calculated values of M_p calculated as described in Sec. II with the choice of $\delta_{pp} = \delta_{pn} = \delta_{np} = \delta_{nn} = 0.35$.

B. Comments on individual experimental data

The following additions and changes have been made to the compilations of Refs. 5 and 6.

(i) The lifetime for the lowest $\frac{9}{2}^+$ level in ^{19}F was taken as the adopted value given by Antilla *et al.*, Ref. 7.

(ii) The lifetime for the lowest $\frac{7}{2}^+$ level in ^{21}Ne was taken from the heavy ion (HI) Doppler shift attenuation method (DSAM) measurement of Warburton *et al.*, Ref. 8.

(iii) The lifetime for the lowest 2^+ level in ^{22}Ne was taken from the HI DSAM measurement of Forster *et al.*, Ref. 9.

(iv) The lifetime for the lowest $\frac{7}{2}^+$ level in ^{23}Na obtained by Smith *et al.*, Ref. 10, was folded in quadrature with the compilation value.

(v) The lifetime of $\tau = 140 \pm 30$ fs for the $\frac{9}{2}^+$ level in ^{23}Mg given by Endt and Van der Leun⁶ from the

TABLE I. Experimental data leading to the $B(E2)$ values as given by Eq. (19) and the theoretical $E2$ matrix elements.

A	J_i	J_f	E_i^{th} (keV)	E_f^{th} (keV)	Z	T_z	E_i^{exp} (keV)	E_f^{exp} (keV)	τ (10^N sec)	N	BR (%)	δ	$M_p = [(2J_i + 1)B(E2)]^{1/2} e \text{ fm}^2$	Theory	References ^a
17	$\frac{1}{2}$	$\frac{5}{2}$	870	0	O	$-\frac{1}{2}$	871	0	258.6 ± 2.6	-12	100		3.55 ± 0.02	2.38	
					F	$+\frac{1}{2}$	500	0	412 ± 9	-12	100		11.26 ± 0.12	9.17	
18	2	0	2000	0	O	-1	1982	0	2920 ± 130	-15	100		6.76 ± 0.15	3.34	
					Ne	+1	1887	0	670 ± 60	-15	100		15.9 ± 0.70	12.9	
18	4	2	3519	2000	O	-1	3555	1982	24.8 ± 1.2	-12	100		5.54 ± 0.14	4.05	
					Ne	+1	3376	1887	4.4 ± 0.6	-12	100		15.1 ± 1.0	15.6	
19	$\frac{5}{2}$	$\frac{1}{2}$	12	0	F	$-\frac{1}{2}$	197	0	128.8 ± 1.5	-9	100		11.3 ± 0.07	10.5	
					Ne	$+\frac{1}{2}$	238	0	26.0 ± 0.8	-9	100		15.6 ± 0.24	15.3	
19	$\frac{9}{2}$	$\frac{5}{2}$	2557	12	F	$-\frac{1}{2}$	2780	197	370 ± 25	-15	100		13.8 ± 0.5	13.3	Ref. 7
					Ne	$+\frac{1}{2}$	2795	238	140 ± 35	-15	100		23.1 ± 2.9	21.5	
19	$\frac{5}{2}$	$\frac{5}{2}$	7561	12	F	$+\frac{1}{2}$	7538	197	113 ± 14	-18	29 ± 3	0.09 ± 0.04	2.2 ± 1.0	2.47	
	$(T = \frac{3}{2})$												1.30 ± 0.15	1.63	
20	2	0	10132	0	Ne	0	10272	0	137 ± 9	-18	0.65 ± 0.14				
	$(T = 1)$														
21	$\frac{5}{2}$	$\frac{3}{2}$	251	0	Ne	$-\frac{1}{2}$	351	0	10.23 ± 0.2	-12	100	0.074 ± 0.004	22.2 ± 1.2	21.2	
					Na	$+\frac{1}{2}$	332	0	10.22 ± 0.12	-12	100	-0.080 ± 0.030	28 ± 10	23.6	
21	$\frac{7}{2}$	$\frac{3}{2}$	1771	0	Ne	$-\frac{1}{2}$	1746	0	74 ± 6	-15	5 ± 1		16.5 ± 1.8	15.9	Ref. 8
					Na	$+\frac{1}{2}$	1716	0	40 ± 15	-15	7 ± 2		27.7 ± 6.5	17.5	
21	$\frac{7}{2}$	$\frac{5}{2}$	1771	251	Ne	$-\frac{1}{2}$	1746	351	74 ± 6	-15	95 ± 1	0.14 ± 0.02	17.5 ± 2.6	21.4	Ref. 8
					Na	$+\frac{1}{2}$	1716	332	40 ± 15	-15	93 ± 2	-0.14 ± 0.03	24.0 ± 6.8	21.8	
22	2	0	1393	0	Ne	-1	1275	0	5.3 ± 0.2	-12	100		15.1 ± 0.3	14.9	Ref. 9
					Mg	+1	1246	0	3.0 ± 1.2	-12	100		21.3 ± 4.2	17.7	
22	4	2	3424	1393	Ne	-1	3357	1275	324 ± 6	-15	100		24.1 ± 0.2	23.6	
					Mg	+1	3308	1246	290 ± 65	-15	100		26.1 ± 2.9	26.0	
23	$\frac{5}{2}$	$\frac{3}{2}$	387	0	Na	$-\frac{1}{2}$	440	0	1600 ± 90	-15	100	-0.058 ± 0.003	25.0 ± 1.5	23.9	
					Mg	$+\frac{1}{2}$	451	0	1800 ± 200	-15	100	0.060 ± 0.020	22.9 ± 7.7	25.0	

TABLE I. (Continued.)

A	J_i	J_f	E_i^{th} (keV)	E_f^{th} (keV)	Z	T_Z	E_i^{exp} (keV)	E_f^{exp} (keV)	τ (10^N sec)	N	BR (%)	δ	$M_p = [(2J_i + 1)B(E2)]^{1/2} e \text{ fm}^2$	Theory	References ^a
23	$\frac{7}{2}$	$\frac{3}{2}$	2154	0	Na	$-\frac{1}{2}$	2076	0	37 ± 3	-15	9 ± 1		20.3 ± 1.4	16.4	Ref. 10
					Mg	$+\frac{1}{2}$	2051	0	80 ± 20	-15	16 ± 2		19.0 ± 2.6	18.1	
23	$\frac{7}{2}$	$\frac{5}{2}$	2154	387	Na	$-\frac{1}{2}$	2076	440	37 ± 3	-15	91 ± 1	-0.19 ± 0.02	21.8 ± 2.4	20.2	Ref. 10
					Mg	$+\frac{1}{2}$	2051	451	80 ± 20	-15	84 ± 2	0.19 ± 0.02	15.1 ± 2.4	21.3	
23	$\frac{1}{2}$	$\frac{5}{2}$	2144	387	Na	$-\frac{1}{2}$	2391	440	800 ± 150	-15	35 ± 1		5.0 ± 0.5	4.87	
					Mg	$+\frac{1}{2}$	2359	451	830 ± 170	-15	69 ± 2		7.3 ± 0.8	7.44	
23	$\frac{9}{2}$	$\frac{5}{2}$	2765	387	Na	$-\frac{1}{2}$	2704	440	110 ± 15	-15	64 ± 1		28.3 ± 1.9	22.2	
					Mg	$+\frac{1}{2}$	2715	451	80 ± 20	-15	68 ± 2		34 ± 4	25.4	Ref. 12
25	$\frac{1}{2}$	$\frac{5}{2}$	723	0	Mg	$-\frac{1}{2}$	585	0	4.88 ± 0.07	-9	100		2.21 ± 0.02	1.92	
					Al	$+\frac{1}{2}$	451	0	3.3 ± 0.05	-9	100		5.13 ± 0.04	4.78	
25	$\frac{3}{2}$	$\frac{5}{2}$	1173	0	Mg	$-\frac{1}{2}$	975	0	16.4 ± 0.9	-12	51 ± 1	-0.36 ± 0.02	3.6 ± 0.2	5.06	
					Al	$+\frac{1}{2}$	945	0	6.2 ± 1.6	-12	44 ± 3	0.34 ± 0.04	5.6 ± 1.0	7.19	
25	$\frac{1}{2}$	$\frac{1}{2}$	1173	723	Mg	$-\frac{1}{2}$	975	585	16.4 ± 0.9	-12	49 ± 1	-0.13 ± 0.03	13.4 ± 3	14.7	
					Al	$+\frac{1}{2}$	945	451	6.2 ± 1.6	-12	56 ± 3	-0.02 ± 0.07	2.0 ± 7	15.5	
25	$\frac{7}{2}$	$\frac{5}{2}$	1749	0	Mg	$-\frac{1}{2}$	1612	0	21 ± 3	-15	100	0.189 ± 0.012	31.4 ± 3	28.7	
					Al	$+\frac{1}{2}$	1612	0	22 ± 7	-15	100	-0.180 ± 0.030	29 ± 7	24.7	
25	$\frac{5}{2}$	$\frac{5}{2}$	2063	0	Mg	$-\frac{1}{2}$	1965	0	1000 ± 400	-15	26 ± 1	0.6 ± 0.1	3.4 ± 0.8	5.56	
					Al	$+\frac{1}{2}$	1790	0	520 ± 70	-15	24 ± 2	-0.82 ± 0.13	7.0 ± 0.9	8.02	
25	$\frac{5}{2}$	$\frac{1}{2}$	2063	723	Mg	$-\frac{1}{2}$	1965	585	1000 ± 400	-15	47 ± 1		21.4 ± 4.3	19.4	
					Al	$+\frac{1}{2}$	1790	451	520 ± 70	-15	38 ± 3		28.9 ± 2.2	19.5	
25	$\frac{5}{2}$	$\frac{3}{2}$	2063	1173	Mg	$-\frac{1}{2}$	1965	975	1000 ± 400	-15	27 ± 1	0.25 ± 0.02	9.0 ± 1.9	10.7	
					Al	$+\frac{1}{2}$	1790	945	520 ± 70	-15	38 ± 3	-0.17 ± 0.01	15.3 ± 1.5	11.0	
25	$\frac{7}{2}$	$\frac{5}{2}$	3015	0	Mg	$-\frac{1}{2}$	2738	0	400 ± 40	-15	6 ± 1	2.9 ± 0.5	2.4 ± 0.2	2.92	
					Al	$+\frac{1}{2}$	2720	0	360 ± 90	-15	8 ± 2	?	3.7	3.93	

TABLE I. (Continued.)

A	J_i	J_f	E_i^{th} (keV)	E_f^{th} (keV)	Z	T_Z	E_i^{exp} (keV)	E_f^{exp} (keV)	τ (10^N sec)	N	BR (%)	δ	$M_p = [(2J_i + 1)B(E2)]^{1/2} e \text{ fm}^2$	Theory	References ^a
25	$\frac{7}{2}$	$\frac{3}{2}$	3015	1173	Mg	$-\frac{1}{2}$	2738	975	400 \pm 40	-15	87 \pm 1		28.9 \pm 1.4	23.8	
					Al	$+\frac{1}{2}$	2720	945	360 \pm 90	-15	77 \pm 3		28.1 \pm 3.6	24.8	
25	$\frac{7}{2}$	$\frac{5}{2}$	3015	2063	Mg	$-\frac{1}{2}$	2738	1965	400 \pm 40	-15	7 \pm 1	-0.47 \pm 0.16	27 \pm 8	6.09	
					Al	$+\frac{1}{2}$	2720	1790	360 \pm 90	-15	15 \pm 2	-0.18 \pm 0.14	11 \pm 8	6.72	
25	$\frac{9}{2}$	$\frac{5}{2}$	3624	0	Mg	$-\frac{1}{2}$	3405	0	10.2 \pm 0.6	-15	19 \pm 1		18.2 \pm 0.7	16.3	
					Al	$+\frac{1}{2}$	3424	0	10 \pm 6	-15	16 \pm 4		16.6 \pm 5.4	13.2	
25	$\frac{9}{2}$	$\frac{7}{2}$	3624	1749	Mg	$-\frac{1}{2}$	3405	1612	10.2 \pm 0.6	-15	81 \pm 1	0.14 \pm 0.02	25.9 \pm 3.7	27.4	
					Al	$+\frac{1}{2}$	3424	1612	10 \pm 6	-15	84 \pm 4	-0.14 \pm 0.03	26 \pm 10	24.2	
26	2	0	2050	0	Mg	-1	1809	0	682 \pm 24	-15	100		17.6 \pm 0.3	16.9	Ref. 13
					Al	0	2069	228	17 \pm 4	-15	4 \pm 1		21.3 \pm 3.7	15.2	
					Si	+1	1796	0	620 \pm 60	-15	100		18.8 \pm 0.9	13.5	Ref. 14
26	2'	0	3250	0	Mg	-1	2938	0	204 \pm 12	-15	10 \pm 1		3.0 \pm 0.2	4.05	Ref. 13
					Si	+1	2783	0	210 \pm 50	-15	31 \pm 3		6.0 \pm 0.7	9.93	Ref. 14
26	2'	2	3250	2050	Mg	-1	2938	1809	204 \pm 12	-15	90 \pm 1	0.12 \pm 0.02	11.8 \pm 2.0	11.6	Ref. 13
					Si	+1	2783	1796	210 \pm 50	-15	69 \pm 3	0.21 \pm 0.10	25 \pm 15	15.2	Ref. 14
26	0'	2	4085	2050	Mg	-1	3588	1809	9500 \pm 600	-15	100		2.19 \pm 0.07	1.28	
					Si	+1	3332	1796	2700 \pm 200	-15	100		5.9 \pm 2.2	3.27	
27	$\frac{1}{2}$	$\frac{5}{2}$	1413	0	Al	$-\frac{1}{2}$	844	0	50 \pm 2	-12	100		8.7 \pm 0.2	7.90	
					Si	$+\frac{1}{2}$	780	0	50 \pm 6	-12	100		10.6 \pm 0.6	10.4	
27	$\frac{3}{2}$	$\frac{5}{2}$	1097	0	Al	$-\frac{1}{2}$	1014	0	2.12 \pm 0.08	-12	97.1 \pm 0.1	0.351 \pm 0.012	12.4 \pm 0.4	14.2	(b)
					Si	$+\frac{1}{2}$	957	0	1.8 \pm 0.2	-12	94 \pm 2	-0.40 \pm 0.14	17 \pm 5	16.7	
27	$\frac{3}{2}$	$\frac{1}{2}$	1097	1413	Al	$-\frac{1}{2}$	1014	844	2.12 \pm 0.08	-12	2.9 \pm 0.1	0.05 \pm 0.06	28 \pm 33	8.96	
					Si	$+\frac{1}{2}$	957	780	1.8 \pm 0.2	-12	6 \pm 2	?	< 840	5.73	
27	$\frac{5}{2}$	$\frac{5}{2}$	3129	0	Al	$-\frac{1}{2}$	2735	0	13 \pm 4	-15	22.1 \pm 1.0	-0.18 \pm 0.06	4.1 \pm 1.5	9.65	
					Si	$+\frac{1}{2}$	2648	0	25 \pm 10	-15	20 \pm 3	0.40 \pm 0.06	6.4 \pm 1.6	10.4	
27	$\frac{5}{2}$	$\frac{1}{2}$	3129	1413	Al	$-\frac{1}{2}$	2735	844	13 \pm 4	-15	1.8 \pm 0.14		16.7 \pm 2.7	17.1	
					Si	$+\frac{1}{2}$	2647	780	25 \pm 10	-15	3 \pm 1		16.1 \pm 4.2	14.8	

TABLE I. (Continued.)

A	J_i	J_f	E_i^{th} (keV)	E_f^{th} (keV)	Z	T_z	E_i^{exp} (keV)	E_f^{exp} (keV)	τ (10^N sec)	N	BR (%)	δ	$M_p = [2J_i + 1]B(E2)^{1/2} e \text{ fm}^2$	Theory	References ^a
27	$\frac{5}{2}$	$\frac{3}{2}$	3129	1097	Al	$-\frac{1}{2}$	2735	1014	13 ± 4	-15	75.7 ± 1.1	-0.115 ± 0.008	15.7 ± 2.7	14.9	
					Si	$+\frac{1}{2}$	2648	957	25 ± 10	-15	77 ± 3	0.083 ± 0.014	8.6 ± 2.3	13.4	
29	$\frac{3}{2}$	$\frac{1}{2}$	1442	0	Si	$-\frac{1}{2}$	1273	0	412 ± 15	-15	100	-0.197 ± 0.009	9.4 ± 0.5	12.2	Ref. 16
					P	$+\frac{1}{2}$	1384	0	200 ± 30	-15	100	0.17 ± 0.02	9.5 ± 1.3	14.3	
29	$\frac{5}{2}$	$\frac{1}{2}$	1917	0	Si	$-\frac{1}{2}$	2028	0	435 ± 15	-15	94 ± 0.5		17.6 ± 0.3	18.8	Ref. 16
					P	$+\frac{1}{2}$	1954	0	360 ± 40	-15	92 ± 1		21.0 ± 1.2	17.5	
29	$\frac{5}{2}$	$\frac{3}{2}$	1917	1442	Si	$-\frac{1}{2}$	2028	1273	435 ± 15	-15	6 ± 0.5	0.03 ± 0.03	1.6 ± 1.6	4.67	Ref. 16
					P	$+\frac{1}{2}$	1954	1384	360 ± 40	-15	8 ± 1	-0.04 ± 0.06	5.4 ± 8.0	3.75	
29	$\frac{3}{2}$	$\frac{1}{2}$	2411	0	Si	$-\frac{1}{2}$	2426	0	25 ± 2	-15	87 ± 1	0.32 ± 0.07	11.2 ± 2.3	8.95	Ref. 16
					P	$+\frac{1}{2}$	2423	0	30 ± 8	-15	84 ± 3	-0.22 ± 0.02	7.1 ± 1.1	5.95	
29	$\frac{3}{2}$	$\frac{5}{2}$	2411	1917	Si	$-\frac{1}{2}$	2426	2028	25 ± 2	-15	0.4 ± 0.1	?	<460	9.72	Ref. 16
					P	$+\frac{1}{2}$	2423	1953	30 ± 8	-15	4 ± 2	?	<260	11.6	
29	$\frac{5}{2}$	$\frac{1}{2}$	3357	0	Si	$-\frac{1}{2}$	3067	0	37 ± 11	-15	3		<4.5	1.17	Ref. 16
					P	$+\frac{1}{2}$	3106	0	33 ± 15	-15	3		<4.5	0.39	
29	$\frac{5}{2}$	$\frac{3}{2}$	3357	1442	Si	$-\frac{1}{2}$	3067	1273	37 ± 11	-15	80 ± 4	-0.26 ± 0.02	19.0 ± 3.2	15.8	Ref. 16
					P	$+\frac{1}{2}$	3106	1383	33 ± 15	-15	76 ± 2	0.25 ± 0.2	21 ± 5	13.4	
30	2	0	2243	0	Si	-1	2235	0	360 ± 20	-15	100		14.2 ± 0.4	16.4	
					P	0	2938	677	95 ± 10	-15	33.2 ± 1.0		15.5 ± 0.9	16.7	Ref. 17
					S	+1	2211	0	233 ± 19	-15	100		18.2 ± 0.8	17.0	Ref. 18
30	2'	0	3797	0	Si	-1	3299	0	83 ± 7	-15	44.7 ± 1.5		6.47 ± 0.29	4.57	
					P	0	4183	677	3.1 ± 0.9	-15	1.3 ± 0.3		5.7 ± 1.1	1.76	Ref. 17
					S	+1	3403	0	158 ± 17	-15	20 ± 3		3.37 ± 0.32	-1.04	Ref. 18
30	2''	0	3190	496	P	0	3834	677	55 ± 20	-15	18 ± 6		6.5 ± 1.6	0.64	
					($T=0$)										
					($T=1$)										
31	$\frac{3}{2}$	$\frac{1}{2}$	1226	0	P	$-\frac{1}{2}$	1266	0	761 ± 47	-15	100	0.30 ± 0.01	10.4 ± 0.5	12.1	Ref. 19
					S	$+\frac{1}{2}$	1249	0	720 ± 180	-15	100	-0.35 ± 0.02	12.8 ± 1.7	12.9	

TABLE I. (Continued.)

A	J_i	J_f	E_i^{th} (keV)	E_f^{th} (keV)	Z	T_Z	E_i^{exp} (keV)	E_f^{exp} (keV)	τ (10^N sec)	N	BR (%)	δ	$M_p = [(2J_i + 1)B(E2)]^{1/2}$ Experiment	Theory	References ^a
39	$\frac{1}{2}$	$\frac{3}{2}$	2500	0	K	$-\frac{1}{2}$	2522	0	75 ± 20	-15	100	0.69 ± 0.13	8.3 ± 1.5	9.16	
					Ca	$+\frac{1}{2}$	2469	0	310 ± 60	-15	100	?	< 8.3	2.38	

^aThe experimental data are taken from the nuclear data compilations, Refs. 5 and 6. Additional recent references are given below.

^bSee text Sec. III A.

experiment by Engmann *et al.*¹¹ is replaced by $\tau = 80 \pm 30$ fs from the experiment of Warburton *et al.*¹² which was not included in the compilation. In connection with our present interest in comparing the transition strengths in mirror nuclei we note that the lifetimes of the $\frac{9}{2}^+$ levels in both ^{23}Mg and ^{23}Na were measured in the same experiment by Warburton *et al.* and thus the relative systematic errors due to stopping power uncertainties (see below) are reduced. The lifetime of $\tau = 110 \pm 20$ fs that Warburton *et al.* obtain for the $\frac{9}{2}^+$ level in ^{23}Na is in good agreement with the compiled average lifetime of 110 ± 15 fs. To improve the accuracy of the extracted isovector matrix elements we strongly recommend that similar experiments be carried out for other pairs of mirror nuclei.

(vi) The lifetimes for the 2^+ levels in ^{26}Mg obtained in the HI DSAM measurement of Dybal *et al.*, Ref. 13, were folded in quadrature with the compilation values.

(vii) The lifetimes for the 2^+ levels in ^{26}Si were taken from the recent HI DSAM measurement of Alexander *et al.*, Ref. 14.

(viii) The mixing ratio for the $^{27}\text{Si} \frac{3}{2}^+ \rightarrow \frac{5}{2}^+$ transition obtained in several experiments⁶ differ by many standard deviations from each other. Sterrenburg and Van Middelkoop¹⁵ have suggested a possible reason for this disagreement and Endt and Van der Leun⁵ have adopted their value, $\delta = -0.50 \pm 0.04$, without averaging previous measurements. We instead adopt an average value with a larger error which encompasses all measurements, $\delta = -0.40 \pm 0.14$.

(ix) The lifetimes of the $\frac{3}{2}^+$ and $\frac{5}{2}^+$ levels in ^{29}Si obtained in the HI DSAM measurements of Scherpenzeel *et al.*, Ref. 16, were folded in quadrature with the compilation values.

(x) The lifetime and branching ratio data for the 2^+ levels in ^{30}P from the recent experiment by Antilla and Keinonen¹⁷ were folded in quadrature with the compilation values.

(xi) The lifetimes of the 2^+ levels in ^{30}S from the HI DSAM measurement of Alexander *et al.*, Ref. 18, were folded in quadrature with the compilation values.

(xii) The adopted values given in Ref. 19 for the lifetimes of the 1.27 and 3.34 MeV levels in ^{31}P are used.

C. General comments

In the present data set many of the $B(E2)$ values, especially those of the proton-rich nuclei, depend on

TABLE II. Lifetimes for the 2.704 MeV $\frac{9}{2}^+$ state in ^{23}Na .

τ (fs)	Error (fs) given by Endt and Van der Leun ^a	Reanalyzed ^g τ (fs)
200±110 ^b	±100	
100 $^{+80}_{-40}$ ^c	±60	
100±25 ^d	±30	
65±15 ^e	±15	102±25
125±30 ^f	±30	
131±10 ^g	±30	
110±20 ^b	±20	
105±20 ⁱ	±20	
110±15 ^j		

^aReference 6.

^fReference 25.

^bReference 22.

^gReference 21.

^cReference 23.

^hReference 12.

^dReference 24.

ⁱReference 26.

^eReference 20.

^jAverage from Ref. 6.

accurate measurements of lifetimes in the range of a few hundred femtoseconds (fs). At present most of the lifetimes in this range can only be measured by the Doppler-shift attenuation method (DSAM). A large fraction of the error on the lifetimes in this method comes from the uncertainty in the stopping power of low-velocity ($\lesssim 2\% v/c$) ions in solids and gases. This systematic error is usually combined in quadrature with the statistical errors. In fact, Endt and Van der Leun⁶ assume a minimum of 15% uncertainty in the lifetimes due to stopping power uncertainties and sometimes the error quoted in the compilation is larger than in the original experimental paper for this reason.

Sometimes the actual error made in the stopping power is larger than the canonical value of 15%. This is illustrated in Table II for the $\frac{9}{2}^+$ level in ^{23}Na . The small value of $\tau = 65 \pm 15$ fs obtained by Meyer *et al.*²⁰ lies outside the average given by Endt and Van der Leun by more than 15%. However, Anttila *et al.*²¹ have reanalyzed the Doppler shift data of Meyer *et al.* using a better calibration of the stopping power parameters and obtain a lifetime of 102 ± 25 fs in agreement with the average. This case may represent an extreme example of the systematic errors which arise in the analysis of DSAM experiments, but it illustrates the basic problem that in some cases the assumption of 15% uncertainty is an underestimate. In contrast to neutron-rich nuclei such as ^{23}Na , the proton-rich

nuclei can be reached by only a few reactions and the possibilities for cross checks are reduced. Thus we feel that the experimental errors on some DSAM lifetimes, especially those for light-ion induced proton-rich transitions, have been underestimated. This may be the reason for some of the disagreements between theory and experiment in Table I, in particular for those involving the $^{25}\text{Al}(\frac{5}{2}^+)_2$, $^{29}\text{P}(\frac{5}{2}^+)_1$, $^{33}\text{Cl}(\frac{7}{2}^+)_1$, and the $^{34}\text{Ar}(2^+)_1$ states.

It would be highly desirable to improve the reliability of the lifetimes in proton-rich nuclei. This might be accomplished by a systematic reanalysis of the DSAM Doppler shift data making use of the best available stopping power theories and experimental stopping power parameters. New experiments could also be performed making use of the higher recoil velocities ($\sim 5\% v/c$) obtainable with light target-heavy beam combinations. At higher recoil velocities the stopping power theory is more reliable. Several such experiments have recently been carried out (Refs. 8, 9, 12, 14, 16, 18, and 19). Also, more experiments are recommended where the lifetimes are measured in both members of the mirror pairs in the same experiment such as in Ref. 12.

D. Isoscalar or isovector dominance?

As can be seen in Table I, the M_p values for only two of the transitions of interest are predicted to change sign as a function of T_Z , the $A=30$ and $A=34$ $2' \rightarrow 0$ transitions. Empirically, however, $|M_p(T_Z)|$ vs T_Z for $T_Z = -1, 0, +1$ is linear for the $A=30$ $2' \rightarrow 0$ transitions, which means that the empirical isoscalar matrix element is significantly larger than predicted and that the empirical isovector matrix element is given by the difference in Eq. (10) (as in the usual case). Thus for the $A=30$ $2' \rightarrow 0$ transition $\Delta M_p(\text{exp}) = -1.55 \pm 0.30$. The situation for the $A=34$ $2' \rightarrow 0$ transition is not clear since the $T_Z=0$ strength is not measured. Thus there are two possibilities $\Delta M_p(\text{exp}) = -1.1 \pm 0.3$ or $+3.8 \pm 0.3$. In the comparisons below both possibilities will be considered. Allowing for an isoscalar correction of $M_0 \lesssim 5 \text{ fm}^2$ for these $2' \rightarrow 0$ transitions it is easy to bring the signs of $\Delta M_p(\text{exp})$ and $\Delta M_p(\text{th})$ into agreement, and the " M_1 " values for these transitions will be treated as negative numbers in the comparison of theory and experiment. Hadron inelastic scattering experiments on ^{34}S would help to determine the relative sign of the proton and neutron matrix elements.

IV. COMPARISON OF EXPERIMENTAL
AND THEORETICAL VALUES OF $E2$
ISOVECTOR MATRIX ELEMENTS
OBTAINED WITH HARMONIC OSCILLATOR
RADIAL WAVE FUNCTIONS

A. Data considered

In discussing the relationship of experimental values of M_1 to the calculations presented here, it is

convenient to define several categories of transitions. Purely from an empirical standpoint, transitions may be classified as to whether or not the isovector matrix element is determined to "useful" accuracy. We have chosen for this criterion an uncertainty limit of $2 e\text{fm}^2$. In Fig. 1 experimental values of M_1 from Table I which meet this accuracy criterion are plotted on the vertical axis and the corresponding theoretical value A_1 on the horizontal axis. If all of the points lie on a straight line it

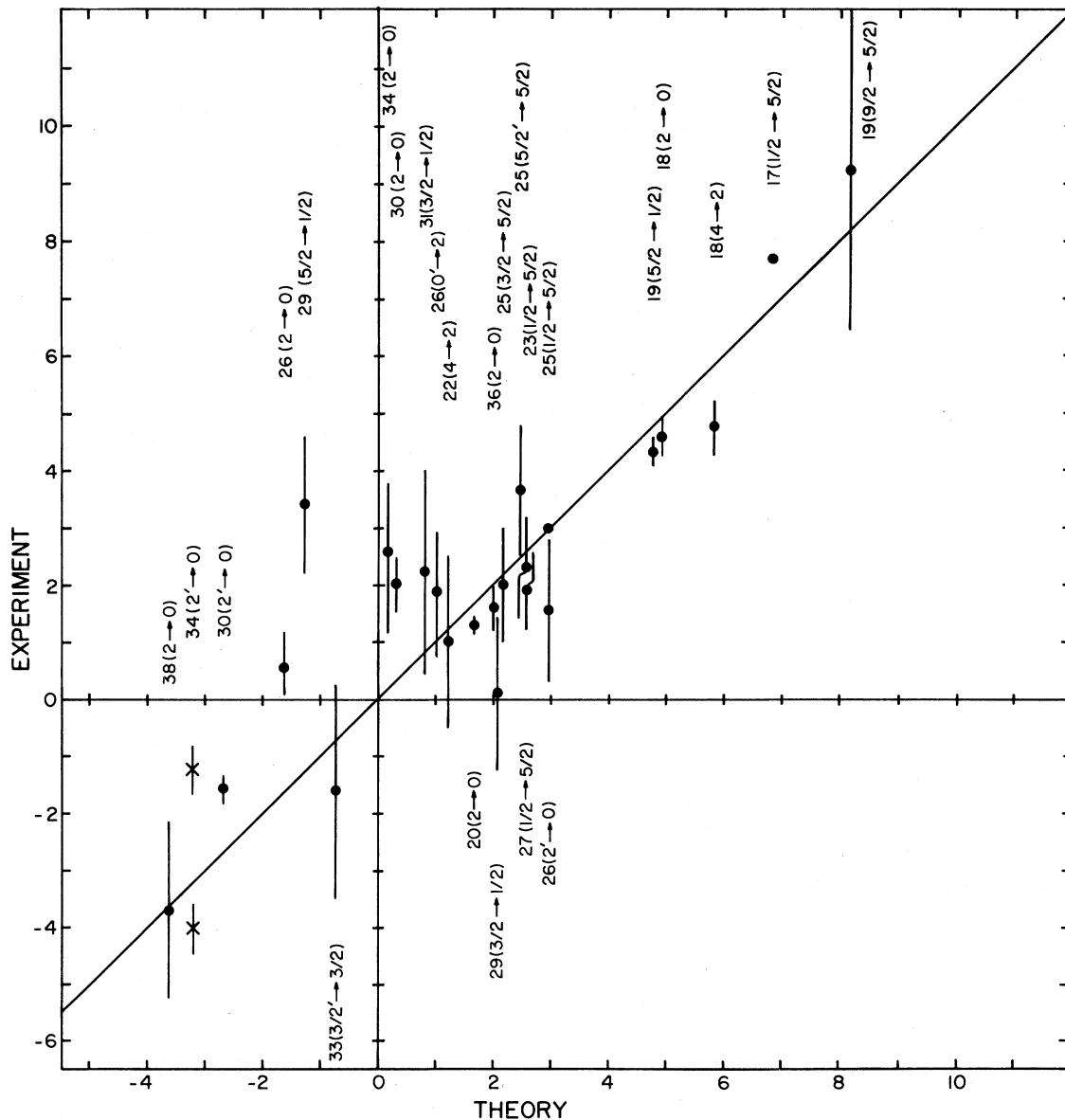


FIG. 1. The experimental differences ΔM_p vs the theoretical matrix element A_1 . As discussed in Secs. II and IV, the points are expected to form a line which passes through the origin with a slope $e_p - e_n$. The line drawn is for the slope $e_n - e_n = 1$. The two crosses for the $A = 34$ ($2' \rightarrow 0$) transition are due to the experimental ambiguity discussed in Sec. III D.

is unlikely that this is accidental, and we can reasonably conclude that the shell model calculation of A_1 is accurate for all of these transitions. In this case the value of the isovector effective charge $e_p - e_n$ is state and mass independent and the numerical value can be obtained from the slope of the line.

The $A = 19, \frac{9}{2}^+ \rightarrow \frac{5}{2}^+$ datum is included in Fig. 1 even though its experimental error exceeds our limit of $2 e \text{ fm}^2$ because it constitutes one of the largest calculated sd -shell isovector matrix elements which is experimentally confirmed. On the other hand the $A = 30, 2_3^+, T = 0 \rightarrow 0_1^+, T = 1$ and $A = 38, 2_1^+, T = 1 \rightarrow 1_1^+, T = 0$ data are not included in Fig. 1 even though their experimental uncertainties ostensibly satisfy our accuracy criterion. These experimental values are quite large in the context of the isovector $E2$ systematics while the corresponding theoretical values are quite small. The theoretical values depend upon the wave functions of $J^\pi = 1^+$ and $2^+ T = 0$ states in double-odd systems and such wave functions typically are not as reliable in detail as are the general run of model states. At the same time, the experimental values upon close analysis do not appear as securely based as are the typical data included in Fig. 1. We conclude that while these data, if correct, may point to significant limitations to the generality of our mode of analysis, their inclusion could contribute a possibly spurious component into our assessment of the dominant trend of the phenomena.

B. Intruder state contamination

From the theoretical standpoint, the entries in Fig. 1 may be classified according to whether the actual nuclear state(s) involved in the transition have the prevailing mapping onto the model wave functions or, rather, appear to contain anomalously large extra-model-space ("intruder state") components. If a transition is significantly contaminated with intruder-state components, its analysis with the present model wave functions will yield results which are incommensurate with the dominant portion of the data. The only state represented in Fig. 1 which appears to have non- $(sd)^n$ components significantly greater than the average run of states considered is the $A = 18, 2_1^+, T = 1$ state. Part of the evidence for its anomalous character is the factor of 2 enhancement of the measured $2^+, T = 1 \rightarrow 0^+, T = 1 M_p$ value over the calculated value. The character of the $2^+, T = 1$ state presumably affects both the $2^+ \rightarrow 0^+$ and $4^+ \rightarrow 2^+$ data.

Nonetheless, the agreement of the theoretical M_1 values of these transitions with experiment is consistent with the general trends of the rest of the data, which may be either accidental or indicative that the isovector transition component is less sensitive to configuration admixtures typical of the shell-crossing excitations than is the isoscalar.

C. Proton binding energy affects

Another criterion by which the entries of Fig. 1 (and Table I) can be classified is the extent to which the experimental state is bound to proton emission. For well bound states, the harmonic-oscillator prescription for single-particle wave functions is not significantly different from, and is stably related to, alternate finite-well prescriptions. As the binding energies become small, however, these prescriptions diverge and the relevance of theoretical estimates based on the harmonic-oscillator prescription becomes questionable. The quantitative specification, let alone the solution, of the problem just qualitatively described is not straightforward. We will discuss the issue in Sec. V. Here we note the general classes of transitions, together with some specific examples, for which these problems should be most acute. The nuclei which consist of an integral number of alpha particles plus a proton have the smallest proton binding energies, ranging from 0.1 to 2.5 MeV. The double-even nuclei with two excess protons are better bound but some states of interest come close in energy to the proton thresholds in these nuclei, which range from 1 to 6 MeV. Specific cases in Fig. 1 which are suspect because of small proton binding energies are the $A = 17 (\frac{1}{2}^+ \rightarrow \frac{5}{2}^+)$, $A = 18 (4^+ \rightarrow 2^+)$, and $A = 25 (\frac{1}{2}^+ \rightarrow \frac{5}{2}^+)$. [The $1s_{1/2}$ proton state is more susceptible to binding energy effects than are the $d_{5/2}$ and $d_{3/2}$ states because of the $l(l+1)$ dependence in the centrifugal barrier.]

D. Apparent discrepancies

The two largest relative discrepancies between theory and experiment evident in Fig. 1 are for the transitions $A = 29 (\frac{5}{2}^+ \rightarrow \frac{1}{2}^+)$ and $A = 34 (2^+ \rightarrow 0^+)$. The $A = 29$ case involves a theoretically negative value of ΔM_p [the $^{29}\text{P } B(E2)$ is calculated to be smaller than that of ^{29}Si] while the experimental magnitudes are reversed. The calculated and measured values of M_p for ^{29}Si agree to within 5% and from this and other evidence there is no obvi-

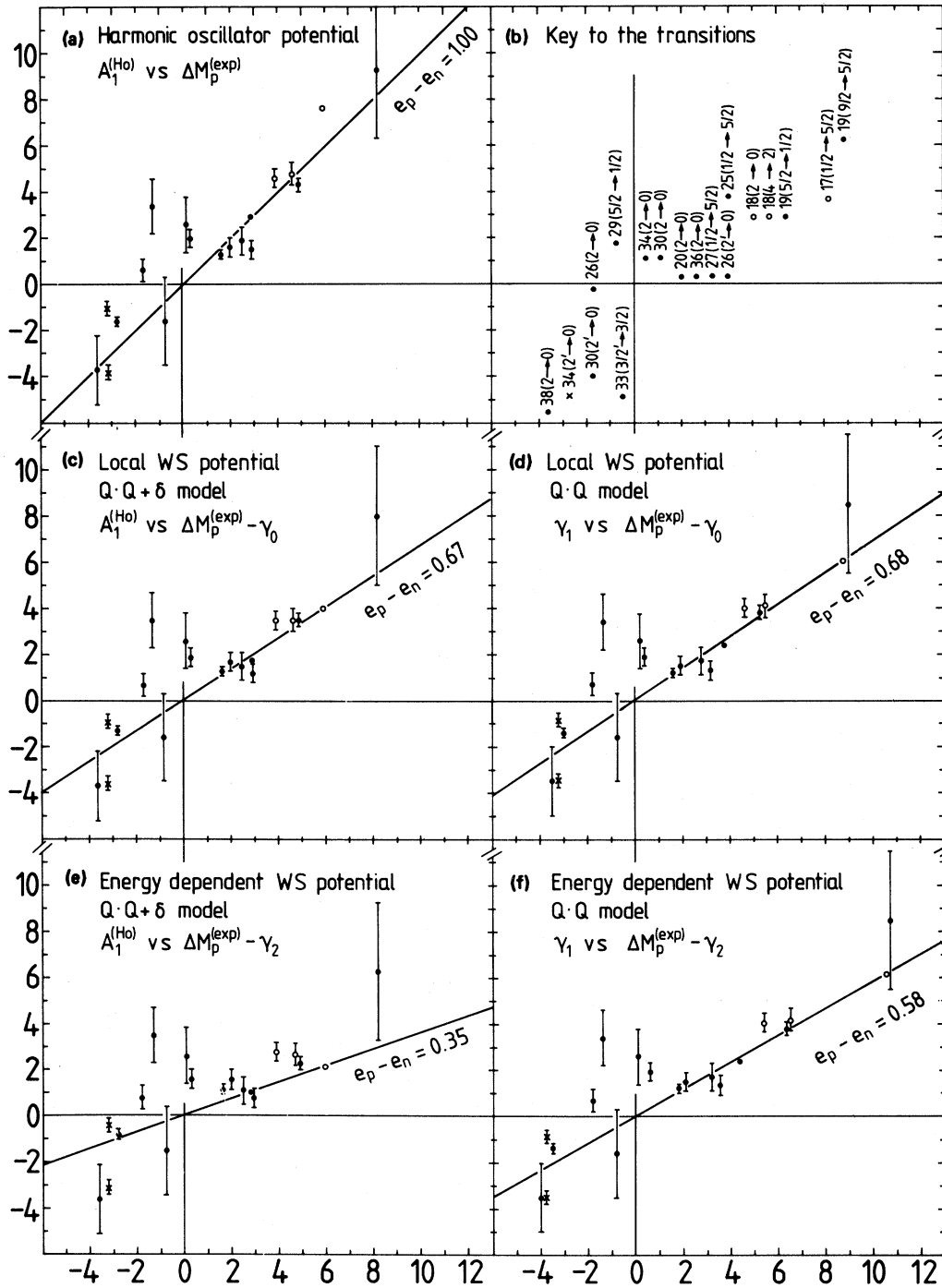


FIG. 2. Plots of experimental and theoretical $E2$ matrix elements for the determination of the isovector effective charge. In all cases the points are expected to lie on a line which passes through the origin and whose slope is $e_p - e_n$. The points in (a) are selected from Fig. 1 which is discussed in Sec. IV. (b) labels the transitions involved in the approximate positions in which they occur in the other figures. (c)–(f) are based on the finite-well potentials and models discussed in Sec. V where γ_0 , γ_1 , and γ_2 are given by Eqs. (29) and (30). The lines in (c)–(f) pass through the $A = 17$ ($\frac{1}{2} \rightarrow \frac{5}{2}$) transition point and the origin. The open circles represent points whose theory is based on the “ZBM” basis discussed in Sec. VD. The two crosses represent the two experimental values for the $A = 34$ ($2' = 0$) transition due to the ambiguity discussed in Sec. IIID.

ous reason to question the general features of the wave functions. Confirmation of the ^{29}P lifetime and/or a test via inelastic scattering seems appropriate before attaching excessive significance to this single instance of "sign reversal." The $A=34$ datum rests on a seemingly well-measured ^{34}S M_p and much less precise ^{34}Cl and ^{34}Ar values which are each two standard deviations larger than the ^{34}S value. Theory predicts a very small isovector term, such that the three isobars should have essentially the same value. There has been a tendency for such differences between neutron-rich and proton-rich systems to diminish with more precise measurements on the proton-rich side.^{14,18}

V. Effects due to the finite-well potential

In this section the important effects due to the differences between harmonic oscillator and finite-well potentials are explored in some detail. In principle, the calculations can be carried out for all transitions considered in Table I; however, for our purpose it will be sufficient to consider the transitions shown in Fig. 2 which are selected because they have small experimental error bars or are interesting because they have negative or large ΔM_p values. The theoretical modifications to the core-polarization charges in finite potentials are discussed in Sec. V A. In Sec. V B a potential which is more general than the usual local Woods-Saxon (WS) form is given and the parameters are discussed in Sec. V C. Finally in Sec. V D a comparison with experiment is made.

A. Modifications to the effective charge model

Equation (11) for the model-space transition matrix element, with the single-particle matrix element written out in terms of its angular and radial integrals, is

$$A_\alpha(T_Z) = \sum_{jj'} D_{\lambda,\alpha}^{T_Z}(jj') \langle j || Y^{(\lambda)} || j' \rangle \langle j | r^\lambda | j' \rangle_\alpha. \quad (20a)$$

The subscript $\alpha = p/n$ on the radial integral indicates the radial wave functions are those of the proton or neutron. It is convenient to rewrite Eq. (20a) in the form

$$A_\alpha(T_Z) = \sum_{jj'} G_\alpha(r^\lambda, jj') A_\alpha^{(\text{HO})}(jj'), \quad (20b)$$

where G is the ratio,

$$G_\alpha(x, jj') = \frac{\langle j | x | j' \rangle_\alpha}{\langle j | x | j' \rangle_{\text{HO}}} \quad (21)$$

and

$$A_\alpha^{(\text{HO})}(jj') = D_{\lambda,\alpha}^{T_Z}(jj') \langle j || Y^{(\lambda)} || j' \rangle \langle j | r^\lambda | j' \rangle_{\text{HO}}. \quad (22)$$

Thus, we will formulate the effects of finite-well depth and the Coulomb potential upon our model-space transition matrix elements in terms of correction factors G which are ratios of the finite-well matrix elements of r^λ to the harmonic oscillator (HO) results for these quantities.

In the harmonic oscillator limit ($G=1$) the proton and neutron radial matrix elements are equal, and hence, as in Sec. II,

$$A_{p/n}^{(\text{HO})}(T_Z=T) = A_{n/p}^{(\text{HO})}(T_Z=-T).$$

However, due to the effects of the Coulomb potential in a well of finite depth the $\langle j | r^\lambda | j' \rangle_p$ are larger than the $\langle j | r^\lambda | j' \rangle_n$ and the equations in Sec. II derived under the assumption that the wave functions have good isospin are not valid; rather Eq. (20) must be evaluated separately for each T_Z value.

For a single-particle (or hole) transition in the model-space ($D_\lambda = \pm 1$) the first-order corrections to A_p can be expressed as a sum over the product of two-body matrix elements and $E2$ matrix elements between proton particle-hole excitations as given, for example, by Eq. (16.72) in Ref. 27. Because of the selection rules for the $E2$ operator (exact in an oscillator model and approximate otherwise) the particle-hole state can only have the $\Delta N=2$ components $(s)^{-1}(sd)^{n+1}$, $(p)^{-1}(sd)^n(fp)^1$, or $(sd)^{n-1}(fdg)^1$. The total matrix element will be a sum over j and j' in the model space of the unrenormalized bare amplitude plus first-order corrections $\delta A_{\alpha'\alpha}$ due to excitations of particle-hole nucleons α' via the valence nucleon α ; e.g., for the proton matrix element

$$M_p = \sum_{jj'} M_p(jj'),$$

where

$$M_p(jj') = A_p(jj') + \delta A_{pp}(jj') + \delta A_{pn}(jj').$$

In the following formulas for M_p the subscript α' on $\delta A_{\alpha'\alpha}$ will be suppressed.

In the many-body valence system $\delta A_\alpha(jj')$ is exactly proportional to $D_\alpha(jj')$, and hence, to $A_\alpha(jj')$

as long as the core excitation connects only to one of the valence particles. The first-order corrections connecting two valence particles (the two-body effective charge²⁸), is relatively small and will be ignored. The remaining orbit and mass dependence in the ratio $\delta A_\alpha(jj')/A_\alpha(jj')$ is related to the nature of the effective residual interaction connecting the valence particle to the particle-hole state of the core. Our aim here is to make as explicit as possible how this state and mass dependence is related to the properties of the valence wave function, in particular to its rms radius. The analytic results which can be obtained with δ function and $Q \cdot Q$ interactions are useful.

For a δ -function residual interaction,^{29,30}

$$\begin{aligned} \frac{\delta A_\alpha^{(\delta)}(jj')}{A_\alpha(jj')} &= \frac{\langle j | k(r) | j' \rangle_\alpha}{\langle j | r^2 | j' \rangle_\alpha} F_\alpha \\ &= \frac{G_\alpha[k(r), jj']}{G_\alpha(r^2, jj')} \delta e_\alpha^{(\delta)}(jj'), \end{aligned} \quad (23)$$

where

$$\delta e_\alpha^{(\delta)}(jj') \equiv \frac{\langle j | k(r) | j' \rangle_{\text{HO}}}{\langle j | r^2 | j' \rangle_{\text{HO}}} F_\alpha \quad (24)$$

and

$$k(r) = r d\rho_g(r)/dr.$$

The constant F_α only depends on α and $\rho_g(r)$ is the ground state proton density. From numerical calculations of the $k(r)$ and r^2 radial integrals with Woods-Saxon wave functions (see Tables 4, 5, and 7 of Ref. 30), we find empirically

$$G_\alpha[k(r), jj'] \approx [G_\alpha(r^2, jj')]^{-1}, \quad (25)$$

and hence

$$\begin{aligned} \delta A_\alpha^{(\delta)}(jj') &\approx A_\alpha(jj') \delta e_\alpha^{(\delta)}(jj') [G_\alpha(r^2, jj')]^{-2} \\ &= A_\alpha^{(\text{HO})}(jj') \delta e_\alpha^{(\delta)}(jj') \\ &\quad \times [G_\alpha(r^2, jj')]^{-1}. \end{aligned} \quad (26)$$

On the other hand, if the effective residual interaction has the form $Q \cdot Q$, where $Q \equiv r^2 Y_\mu^{(2)}$, δA can be obtained by putting $k(r) = r^2$ in Eq. (23) and an effective charge which is completely state independent can be defined,

$$\begin{aligned} \delta A_\alpha^{(Q \cdot Q)}(jj') &= A_\alpha(jj') \delta e_\alpha \\ &= A_\alpha^{(\text{HO})}(jj') \delta e_\alpha G_\alpha(r^2, jj'). \end{aligned} \quad (27)$$

The effective charge $\delta e^{(\delta)}$ depends not only on j and j' but also on mass number through the depen-

dence of $\rho_g(r)$ in Eq. (24) on mass. The state and mass dependence of the effective charge obtained with the Kuo-Brown G -matrix interaction is very close to that of $\delta e^{(\delta)}$; compare in Ref. 30 the $\delta e^{(\delta)}$ given in Table I and the δe^{micr} give in Tables 10 and 11. In both cases the effective charges are expected to increase by a factor of 2 in going from $A = 17$ to $A = 39$. However, it is found empirically that the isoscalar effective charges are to good accuracy state and mass independent. This is apparent from the agreement between theory and experiment in Tables I and V, where the effective charges utilized in the theory have been assumed *ab initio* to be state and mass independent. This suggests that the effective interaction $Q \cdot Q$ is more realistic and we will concentrate in the discussion on results based on Eq. (27). Also, because it lends itself to a simple graphical representation of experiment versus theory, we will utilize a model which lies between the δ and $Q \cdot Q$ results of Eqs. (26) and (27) which we will call " $Q \cdot Q + \delta$."

$$\delta A_\alpha^{(Q \cdot Q + \delta)}(jj') = \delta A_\alpha^{(\text{HO})}(jj') \delta e_\alpha, \quad (28)$$

where for simplicity the state and mass dependence of δe_α will be ignored.

Summing over j and j' and taking the difference ΔM_p defined by Eq. (9), the following linear equations in $e_p - e_n$ can be obtained

$$\Delta M_p^{(Q \cdot Q)} = (e_p - e_n) \gamma_1 + \gamma_0 \quad (29a)$$

and

$$\Delta M_p^{(Q \cdot Q + \delta)} = (e_p - e_n) \Delta A_p^{(\text{HO})} + \gamma_2, \quad (30a)$$

where

$$\gamma_0 = \frac{[\Delta A_p + \Delta A_n]}{2} (e_p + e_n), \quad (29b)$$

$$\gamma_1 = \frac{[\Delta A_p - \Delta A_n]}{2}, \quad (29c)$$

$$\gamma_2 = [\Delta A_p - \Delta A_p^{(\text{HO})}], \quad (30b)$$

and

$$\Delta A_\alpha = [A_\alpha(T_Z = T) - A_\alpha(T_Z = -T)] / \Delta T_Z.$$

In the harmonic oscillator limit $\Delta A_p^{(\text{HO})} = -\Delta A_n^{(\text{HO})} = \Delta A_1^{(\text{HO})}$ and Eqs. (18), (29a), and (30a) are identical. The quantity γ_0 has been calculated with $e_p + e_n = 1.7$ and is usually small (less than 0.2 fm²) except for $A \leq 19$.

B. Form of the potential

The Skyrme-type two-body interactions used in Hartree-Fock calculations for spherical nuclei³¹⁻³³

$$-\frac{\hbar^2}{2m} \frac{d^2}{dr^2} \Psi_L(r) + \frac{\hbar^2}{2m} \frac{l(l+1)}{r^2} \Psi_L(r) + V_L(r, \epsilon_s) \Psi_L(r) = \epsilon_s \Psi_L(r), \quad (31)$$

where

$$V_L(r, \epsilon_s) = [1 - m^*(r)/m] \epsilon_s + V_0(r) \pm \frac{(N-Z)}{A} V_1(r) + V_{so}(r) \langle \underline{l} \cdot \underline{\sigma} \rangle + V_{Coul}(r), \quad (32)$$

$$\frac{m^*(r)}{m} = \{1 + C_0[\rho_p(r) + \rho_n(r)] \pm C_1[\rho_p(r) - \rho_n(r)]\}^{-1}, \quad (33)$$

and

$$\Psi_s(r) = [m^*(r)/m]^{1/2} \Psi_L(r). \quad (34)$$

In these equations the \pm refers to the potential for protons/neutrons.

In terms of the Skyrme parameters t_1 and t_2 the coefficients in Eq. (33) are given by

$$C_0 = \frac{2m}{\hbar^2} \left[\frac{5t_2 + 3t_1}{16} \right], \quad (35)$$

$$C_1 = \frac{2m}{\hbar^2} \left[\frac{t_2 - t_1}{16} \right].$$

The potentials V_0 , V_1 , and V_{so} can also be expressed in terms of the densities and the Skyrme parameters. However, here we will assume a Woods-Saxon form for these (for the present results V_1 does not enter since $N=Z$), so that

$$V_0(r) = U_0 \{1 + \exp(r - r_0 A^{1/3})/a_0\}^{-1} \quad (36a)$$

and

$$V_{so}(r) = U_{so} \frac{1}{r} \frac{d}{dr} \times \{1 + \exp(r - r_{so} A^{1/3})/a_{so}\}^{-1}. \quad (36b)$$

The spin-orbit parameters were fixed at $V_{so} = 12$ MeV, $r_{so} = r_0$, and $a_{so} = a_0$. The Coulomb potential was derived from the standard uniform density approximation [Eq. (25) in Ref. 30].

The form of Eq. (32) implies a self-consistent

lead to a spherical nonlocal potential with eigenfunctions $\Psi_s(r)$ and eigenvalues ϵ_s which can be obtained from the following equivalent equation which involves a local energy-dependent potential³³

iteration since $m^*(r)$ depends on $\rho(r)$ which itself depends on the potential. However, it is sufficiently accurate to replace the $\rho(r)$ needed for $m^*(r)$ by Fermi distributions which are constrained to give the experimental rms radii and to have a diffuseness of 0.5 fm.

In the limit when $m^*(r)/m = 1$ Eq. (32) goes into the local Woods-Saxon potential. In nuclear matter $m^*(r)/m$ is less than unity due to the nonlocality of the two-body interaction and realistic two-body interactions³⁴ give a nuclear matter value of $m^*/m = 0.6-0.7$. However, in finite nuclei there are additional corrections due to coupling with core vibrations which tend to increase m^*/m .³⁵ It is theoretically expected that m^*/m increases to near unity for single-particle states near the Fermi surface and smoothly goes to the nuclear matter value for deep hole states. Empirically this has not been confirmed for a given nucleus. The most that is known is that $m^*/m \approx 0.6$ is required for deep holes states in *light nuclei* (see below and Table III) and that $m^*/m \approx 1.0$ is required for states near the Fermi surface in *heavy nuclei* (such as ²⁰⁸Pb). Since we do not know how to solve the Schrödinger equation when $m^*(r)/m$ itself depends on energy, results for two different types of potentials will be presented: for a "local WS potential" when $m^*/m = 1$ ($C_0 = 0$), and for an "energy dependent WS potential" which has $m^*(r=0)/m \approx 0.6$ with C_0 obtained from the parameters $t_1 = 572$ MeV fm⁵ and $t_2 = -32.8$ MeV fm⁵ which belong to the continuous family of Skyrme potentials obtained by Beiner *et al.*³²

C. Parameters of the potentials

Parameters of both the "energy dependent" and "local" WS potential are chosen independently for the "closed shell" nuclei ¹⁶O and ⁴⁰Ca to reproduce the properties discussed below. Then a simple interpolation is used to obtain their parameters for other *sd* shell nuclei.

For $N=Z$ nuclei there are four parameters to be determined: U_0 , r_0 , a_0 [Eq. (36)], and C_0 [Eq. (35)].

TABLE III. Single-particle properties of ^{16}O and ^{40}Ca .

	^{16}O			Exp	^{40}Ca			Exp	
	Potential		Energy		Potential		Energy		
	Harmonic oscillator	Local WS	Energy dependent WS		Harmonic oscillator	Local WS	Energy dependent WS		
(A) Properties of the charge distribution									
$\langle r^2 \rangle^{1/2}(\text{fm})$	2.726	2.716	2.716	2.720(4) ^a	$\langle r^2 \rangle^{1/2}(\text{fm})$	3.479	3.477	3.477	3.483(3) ^b
$\langle r^2 \rangle^{1/4}(\text{fm})$	3.018	3.038	3.038	3.04(4) ^b	$\langle r^4 \rangle^{1/4}(\text{fm})$	3.810	3.831	3.831	3.83(4) ^b
$\rho(r=0) (\text{fm}^{-3})$	0.071	0.067	0.080	0.075(2) ^b	$\rho(r=0) (\text{fm}^{-3})$	0.106	0.097	0.097	0.088(2) ⁱ
(B) Neutron single-particle rms radii (fm)									
$0s_{1/2}$	2.17	2.08	1.94		$0s_{1/2}$	2.40	2.42	2.30	
$0p_{3/2}$	2.80	2.69	2.71		$0p_{3/2}$	3.10	3.03	2.95	
$0p_{1/2}$	2.80	2.68	2.77		$0p_{1/2}$	3.10	2.99	2.92	
$0d_{5/2}$	3.31	3.49 ^c	3.69 ^c	3.46(12) ^e	$0d_{5/2}$	3.67	3.54	3.57	
$1s_{1/2}$	3.31	4.17 ^d	4.56 ^d	4.20(15) ^e	$0d_{3/2}$	3.67	3.51	3.61	
					$1s_{1/2}$	3.67	3.57	3.75	
					$0f_{7/2}$	4.16	4.06 ^l	4.28 ^l	3.89(12) ^k
					$1p_{3/2}$	4.16	4.44 ^m	4.79 ^m	4.27(8) ^k
(C) Proton single-particle energies (MeV)									
$0s_{1/2}$	27.9	42.1	42(10) ^f		$0s_{1/2}$	31.2	50.5	46–58 ^f	
$0p_{3/2}$	14.9	18.1	18.4 ^g		$0p_{3/2}$	21.7	32.3	26–42 ^f	
$0p_{1/2}$	11.6	13.4	12.1 ^g		$0p_{1/2}$	19.9	28.7		
$0d_{5/2}$	1.9	0.6	0.6 ^g		$0d_{5/2}$	11.5	15.3		17 ^f
$1s_{1/2}$	0.1	0.1	0.1 ^g		$0d_{3/2}$	7.9	8.8	8.3 ^g	
					$1s_{1/2}$	8.6	10.6	10.9 ^g	
					$0f_{7/2}$	1.1	1.1	1.1 ^g	

^aReference 36.^bReferences 37 and 38.^cThe potential depth was adjusted slightly to reproduce the $0d_{5/2}$ binding energy of 4.14 MeV.^dBE ($1s_{1/2}$) = 3.27 MeV reproduced (see c).^eReference 39 and Table 14 in Ref. 40.^fReference 41.^gBased on the binding energies of the lowest levels of each spin in $A = A_c \pm 1$ nuclei with $A_c = 16$ or 40.^hReference 42.ⁱReference 43.^kReference 44.^lBE ($0f_{7/2}$) = 8.36 MeV reproduced (see c).^mBE ($1p_{3/2}$) = 6.42 MeV reproduced (see c).

For the two choices of the values of m^*/m or C_0 discussed above in Sec. VB, the remaining three parameters were chosen to reproduce exactly the $\langle r^2 \rangle^{1/2}$ and $\langle r^4 \rangle^{1/4}$ charge radii and the binding energy of one valence proton orbit ($1s_{1/2}$ for ^{16}O and $0f_{7/2}$ for ^{40}Ca). The charge density is related to that of the point nucleons as described in Ref. 40. Some properties of ^{16}O and ^{40}Ca obtained with these potentials are given in Table III.

The energies of the deep hole states are in much better agreement with an energy dependent potential

(WSE) than with the local potential (WSL). Relative to the WSL potential, the WSE potential yields deeper binding, and hence smaller rms radii of the inner orbits. Consequently, it also yields valence orbits which have relatively larger rms radii, in order that the average rms remain the same. These larger valence radii from the WSE potential are, however, too large compared to the values obtained for valence neutron radii from analyses of sub-Coulomb one-nucleon transfer reaction experiments (see Table III). The local potential gives valence radii in much

TABLE IV. Calculated and experimental rms charge radii (fm).

Exp	Fixed $A \rightarrow A-1$ separation energy			
	WSL ^a potential	WSE ^b potential	WSL ^a potential	WSE ^b potential
¹⁶ O	2.720(4) ^c	2.716	2.716	2.716
²⁰ Ne	3.020(20) ^d	3.001	3.035	2.871
²⁴ Mg	3.035(18) ^d	3.130	3.169	3.009
²⁸ Si	3.125(3) ^d	3.238	3.258	3.147
³² S	3.263(2) ^d	3.336	3.354	3.266
³⁶ Ar	3.399(5) ^d	3.411	3.421	3.365
⁴⁰ Ca	3.483(3) ^e	3.477	3.477	3.477

^aLocal Woods-Saxon.

^bEnergy dependent Woods-Saxon.

^cReference 36.

^dSee Table III in Ref. 4.

^eReference 42.

better agreement with these data but deep hole states which are not bound enough. (Comparison with these valence radii is important of course because the model-space $E2$ matrix elements are directly proportional to the valence rms radii.) At present we cannot resolve these inconsistencies and will take two points of view:

(i) The energy dependent potential is correct and there is at present some unknown problem in the method of extracting valence radii values from one-nucleon transfer data.

(ii) The energy dependent potential is incorrect for reasons that may be related to the effects of core excitations, and hence, one should use the local potential simply because it gives fairly good agreement with valence radii obtained from one-nucleon transfer.

The parameters of the potential turn out to be similar for ¹⁶O and ⁴⁰Ca with the WSE potential (U_0, r_0, A_0) = (49.0, 1.27, 0.64) for ¹⁶O and (48.3, 1.27, 0.76) for ⁴⁰Ca. With the WSL potential (U_0, r_0, a_0) = (49.6, 1.31, 0.53) for ¹⁶O and (52.4, 1.26, 0.72) for ⁴⁰Ca. The extrapolation to other sd shell nuclei was obtained with a mass dependence for $X = U, r$ or a given by

$$X_0 = X_a + X_b A^{-1/3}. \quad (37)$$

The radial wave functions were calculated with the local (WSL) and energy dependent (WSE) Woods-Saxon potential parameters for the even-even $N=Z$ sd shell nuclei. The rms charge radii for these nuclei are compared with experiment in Table IV. The total point densities used for the charge distribution were obtained by weighting the

radial probability distribution of each orbit by the ground state ($0d_{5/2}, 1s_{1/2}, 0d_{3/2}$) occupation numbers calculated with the Chung-Wildenthal wave functions (the occupations in the lower and higher major shells were assumed to be $2j+1$ and 0, respectively). The calculated rms radii are systematically larger than experiment for both WSL and WSE potentials. The main reason for this is that the eigenenergies of the spherical potential represent the Hartree-Fock *centroid* energy of all $(sd)^n$ configurations which are typically spread over several hundred MeV. Because of correlations the ground states in the $N=Z$ open shell nuclei are more tightly bound and hence the rms radius is smaller. The effect of this can be estimated by adjusting the spherical potential depths to reproduce the binding energy difference between ground state of the nucleus with mass A and the centroid of levels in the $A-1$ nuclei whose summed spectroscopic factors for a given nlj value is the occupation number. The results of such calculations⁴⁵ are shown in the last two columns of Table IV. For both WSL and WSE potentials the rms radii are significantly reduced and brought into fairly good agreement with experiment.

Similarly, for the $E2$ transitions each $[a_j^\dagger \times a_{j'}]$ in Eq. (13) can be factored into $A \rightarrow A-1$ fractional parentage coefficients [e.g., Eq. (14.22) in Ref. 27] to determine the appropriate separation energies for j and j' . However, to actually carry this out for all of the transitions we consider at present is much too laborious. Rather in most cases the transitions in the nuclei $A-1, A+1,$ and $A+2$ are calculated with the radial wave functions obtained with the spherical potential for the even-even nucleus A . Two exceptions are made in cases where the transi-

TABLE V. E2 Matrix elements with finite-well potentials.

$J_i \rightarrow J_f$	A,Z	Harmonic oscillator		Potential Local		Energy dependent		Exp ^b	Theory ^c	
		A_p (fm ²)	A_n (fm ²)	A_p (fm ²)	A_n (fm ²)	A_p (fm ²)	A_n (fm ²)	M_p (fm ²)	M_p (fm ²)	M_n (fm ²)
$\frac{1}{2} \rightarrow \frac{5}{2}^a$	¹⁷ O	0.6	6.5	0.8	8.4	1.0	10.5	3.55(2)	4.7	10.0
	¹⁷ F	6.5	0.6	10.5	0.7	12.4	0.9	11.26(12)	12.4	5.5
$2 \rightarrow 0^a$	¹⁸ O	2.6	10.4	3.3	11.4	3.7	13.5	6.8(2)	8.9	14.6
	¹⁸ Ne	10.4	2.6	13.2	2.8	15.1	3.3	15.9(7)	16.4	9.2
$4 \rightarrow 2^a$	¹⁸ O	0.4	9.8	0.5	10.7	0.6	12.7	5.5(2)	5.4	12.5
	¹⁸ Ne	9.8	0.4	12.4	0.4	14.2	0.5	15.1(10)	14.4	6.0
$\frac{5}{2} \rightarrow \frac{1}{2}$	¹⁹ F	5.2	10.0	6.2	10.6	7.4	13.0	11.3(7)	11.9	15.0
	¹⁹ Ne	10.0	5.2	11.8	5.5	14.2	6.8	15.6(2)	16.1	11.6
$\frac{9}{2} \rightarrow \frac{5}{2}$	¹⁹ F	6.2	14.3	7.2	15.0	8.6	18.1	13.8(5)	15.0	20.5
	¹⁹ Ne	14.3	6.2	16.6	6.5	19.7	7.9	23(3)	22.1	14.9
$2 \rightarrow 0$	²⁰ Ne	1.6	-1.6	1.7	-1.5	1.8	-1.7	1.30(15)	1.3	-1.0
$T=1 \rightarrow 0$										
$\frac{1}{2} \rightarrow \frac{5}{2}$	²⁵ Mg	0.54	3.40	0.61	4.06	0.65	4.67	2.21(2)	2.5	4.9
	²⁵ Al	3.40	0.54	4.63	0.58	5.33	0.62	5.13(4)	5.6	2.8
$2 \rightarrow 0$	²⁶ Mg	10.7	7.3	11.9	7.7	13.1	8.8	17.6(3)	17.1	14.2
	²⁶ Si	7.3	10.7	8.2	11.2	9.3	12.4	18.8(9)	14.5	16.6
$2' \rightarrow 0$	²⁶ Mg	1.2	7.0	1.3	7.4	1.5	8.3	3.0(2)	4.9	9.1
	²⁶ Si	7.0	1.2	7.9	1.2	8.8	1.4	6.0(7)	9.6	4.9
$\frac{1}{2} \rightarrow \frac{5}{2}$	²⁷ Al	4.1	6.7	4.6	7.0	4.9	7.8	8.7(2)	8.4	10.1
	²⁷ Si	6.7	4.1	7.4	4.3	8.2	4.7	10.6(6)	10.5	8.3
$\frac{5}{2} \rightarrow \frac{1}{2}$	²⁹ Si	11.4	10.0	12.4	10.4	13.9	11.8	17.6(3)	19.0	17.5
	²⁹ P	10.0	11.4	11.1	11.7	12.5	13.2	21.0(12)	18.0	18.5
$2 \rightarrow 0$	³⁰ Si	9.6	10.2	10.3	10.4	11.5	12.0	14.2(4)	16.6	16.6
	³⁰ S	10.2	9.6	11.2	9.8	12.8	10.9	18.2(8)	17.2	16.3
$2' \rightarrow 0$	³⁰ Si	-3.9	1.8	-4.2	1.9	-4.8	2.3	6.5(3)	-4.0	0.3
	³⁰ S	1.8	-3.9	2.0	-3.9	2.5	-4.5	3.4(3)	0.6	-3.6
$\frac{3}{2}' \rightarrow \frac{3}{2}$	³³ S	5.0	4.2	5.2	4.2	5.8	4.7	10.2(9)	7.8	7.4
	³³ Cl	4.2	5.0	4.4	4.9	5.0	5.5	8.6(17)	7.3	7.6
$2 \rightarrow 0$	³⁴ S	8.2	8.5	8.6	8.4	9.6	9.3	14.0(3)	13.7	13.5
	³⁴ Ar	8.5	8.2	8.9	8.0	9.1	9.9	21(3)	13.8	13.2
$2' \rightarrow 0$	³⁴ S	3.0	-3.3	3.3	-3.3	3.9	-3.7	4.9(2)	2.3	-2.3
	³⁴ Ar	-3.3	3.0	-3.5	3.0	-3.9	3.6	2.8(5)	-2.6	1.9
$2 \rightarrow 0$	³⁶ Ar	2.0	-2.0	2.0	-1.9	2.1	-2.0	1.6(4)	1.4	-1.3
$T=1 \rightarrow 0$										
$2 \rightarrow 0$	³⁸ Ar	7.3	0	7.3	0	7.6	0	11.2(3)	8.3	3.3
	³⁸ Ca	0	7.3	0	6.9	0	7.2		3.1	7.9

^aObtained with the "ZBM" basis, see text, Sec. V D.

^bFrom Table I.

^cLocal potential and "Q·Q" model with $e_p = 1.15$ and $e_n = 0.45$. $M_p = A_p e_p + A_n e_n$ and $M_n = A_p e_n + A_n e_p$.

tions are particularly sensitive to separation energy and have relatively very small experimental errors:

(i) The $A = 17 \frac{1}{2}^+ \rightarrow \frac{5}{2}^+$ transitions were calculated with proton and neutron separation energies based on the experimental binding energy differences between the $A = 17$ and the ^{16}O ground state.

(ii) The $A = 25 \frac{1}{2}^+ \rightarrow \frac{5}{2}^+$ transitions were calculated with proton and neutron separation energies based on the experimental binding energy differences between the $A = 25$ states and the ^{24}Mg ground state, since the ^{24}Mg ground state accounts for most of the $A \rightarrow A - 1$ fractional parentage of these states.

D. Comparison of experiment and theory

The radial wave functions obtained as described in Sec. VC are combined with the coefficients $D_\lambda(jj')$ as in Eq. (20) to obtain the amplitudes $A_\alpha(T_Z)$ given in Table V. In order to obtain an x - y plot that is linear in $(e_p - e_n)$, these amplitudes are combined according to Eqs. (29) and (30) and then plotted (in Fig. 2) in the form γ_1 vs $\Delta M_p^{(\text{exp})} - \gamma_0$ for the “ $Q \cdot Q$ ” model, and $\Delta A_p^{(\text{HO})}$ vs $\Delta M_p^{(\text{exp})} - \gamma_2$ for the “ $Q \cdot Q + \delta$ ” model.

Given the large weight of the $A = 17$ and 18 transitions in determining the isovector effective charge, effects due to admixtures of nonclosed shell components of the ^{16}O core (beyond the $\Delta N = 2$ excitations taken into account by the effective charge) have been estimated. The coefficients D_λ were calculated in a complete basis of $(0p_{1/2}, 0d_{5/2}, 1s_{1/2})^5$ using the Reehal-Wildenthal interaction.⁴⁶ This basis will be referred to as the “ZBM” (Zucker, Buck, and McGrory⁴⁷) basis. The ZBM basis provides a good description of the low lying states in ^{16}O with configurations up to 4p-4h relative to the closed shell. The D_λ coefficients involving the $0d_{3/2}$ orbit were taken from the sd shell calculations. The matrix elements A_α in the ZBM and sd basis are compared in Table VI. In Fig. 2 points obtained with the ZBM calculations are shown with open circles. The differences between the sd and ZBM results for the isovector matrix elements is not very large, as can be seen by comparing Figs. 1 and 2, and these effects will even be less important for $A \geq 19$.

For the data in Fig. 2 we have not attempted to make a least squares fit to $e_p - e_n$. Rather we simply show the lines corresponding to the values for $e_p - e_n$ which match the $A = 17 \frac{1}{2}^+ \rightarrow \frac{5}{2}^+$ transition. The agreement between experiment and

TABLE VI. Comparison between sd shell and “ZBM” model-space amplitudes (harmonic-oscillator radial wave functions).

		sd		ZBM	
		A_p (fm ²)	A_n (fm ²)	A_p (fm ²)	A_n (fm ²)
$\frac{1}{2} \rightarrow \frac{5}{2}$	^{17}O	0	6.8	0.6	6.5
$2 \rightarrow 0$	^{18}O	0	9.6	2.6	10.4
$4 \rightarrow 2$	^{18}O	0	11.6	0.4	9.8

theory is a little better with the finite well potentials than with the harmonic oscillator but it is clearly not easy to judge which finite well potential or model is best.

The four transitions $A = 26 (2 \rightarrow 0)$, $A = 29 (\frac{5}{2} \rightarrow \frac{1}{2})$, $A = 30 (2 \rightarrow 0)$, and $A = 34 (2 \rightarrow 0)$ are always in relatively poor agreement with theory and hopefully future improvements in the experimental situation, or future modifications to the theory, will resolve these discrepancies. The most significant improvement in going to the finite well potentials and the resulting smaller isovector effective charge is in the agreement for the $A = 30 (2' \rightarrow 0)$ transition. As discussed in Sec. III D, there is an ambiguity about which sign to use in Eq. (10) for the $A = 34 (2' \rightarrow 0)$ transition resulting in two values both of which are shown in Fig. 2. The smaller value is in better agreement with the systematics.

VI. DISCUSSION AND CONCLUSIONS

The present study has utilized experimentally measured strengths of electric quadrupole transitions between matched pairs of levels in isobaric analog nuclei of the sd shell in an attempt to determine the basic properties of isovector $E2$ phenomena in the low-excitation region of light nuclei. As we have discussed, the requirements for extracting useful information on isovector $E2$ strengths from the raw data are (1) enough data, of good precision, to establish unambiguous trends and (2) a theory adequate to understand the underlying foundations of the experimental observations.

Our theoretical analysis naturally factors into three components: (1) many-body configuration-mixed shell-model predictions for the microscopic one-body transition densities, (2) a theoretical description for the radial wave functions of the model-space nucleons, and (3) an overall scale factor, the isovector effective charge, which serves to

renormalize the model-space result for the omission of many highly excited configurations so that absolute agreement with experiment is obtained.

There is some uncertainty in the theoretical description for the radial wave functions associated with the effective mass or the energy dependence of the potential. As discussed in Sec. V conventional Hartree-Fock theory predicts rms valence neutron radii in ^{17}O which are too large compared with those deduced from analysis of sub-Coulomb one-nucleon transfer reactions. Ideas have been proposed which may explain this discrepancy³⁵ but they have yet to be developed to a stage for practical application. Given this situation we have made comparisons on two levels. First, *all* matrix elements were calculated with harmonic-oscillator wave functions with a radius parameter which is the same for all neutrons and protons within an isobaric multiplet but which is determined independently for each mass value by fitting to the measured rms charge radius of the most stable nucleus in each mass chain.⁴ Second, a selected number of matrix elements were calculated with two types of finite-well potentials; an energy dependent potential which has a realistic (conventional) effective mass and a local potential which does not have a realistic effective mass but does reproduce the valence neutron rms radii.

The analysis we have presented divides into two levels. On the first the configuration mixed shell-model predictions can be tested by the harmonic oscillator calculations with an empirical isovector effective charge that turns out to be $e_p - e_n = 1.0$. These results are given in Table I, plotted in Fig. 1, and discussed in Sec. IV. On this level the experimental $E2_{IV}$ matrix elements are reproduced remarkably well, with some exceptional cases which may be due to the experimental uncertainties discussed in detail in Secs. III and IV.

On the second level we have focused on the "best" value for the isovector effective charge. We note that the theoretical isovector effective charge is dependent on the radial wave functions as well as what is assumed about the "radial dependence" of the effective $E2$ operator. Owing to the radial dependence in the effective operator, variations of as much as a factor of 2 between different orbits and different masses in the sd shell are found with calculations based on realistic two-body interactions. (See, for example, Tables 10 and 11 in Ref. 30.) However, the empirical effective charge, as deduced from the strong transitions in nuclei with $A \geq 19$, varies from a constant by less than about

10%. This can be seen by comparing the theoretical M_p values based on constant values for e_p and e_n with the experimental values in Tables I and V. This implies that the radial dependence of the effective $E2$ operator is the same as that of the bare operator, namely r^2 . This result would naturally arise if the effective interaction has the form $Q \cdot Q$. We will base our main conclusions on the $Q \cdot Q$ model. For comparison, in Sec. V A in Fig. 2 a formulation and results based on a model which is intermediate between a short range and $Q \cdot Q$ interaction, the $Q \cdot Q + \delta$ model, are also given.

From Figs. 2(d) and (f) it can be seen that most experimental data are, within experimental error, consistent with a constant isovector effective charge of 0.68(0.58) with the local (energy-dependent) potential. We suggest that the deviation for $A = 29$ may be due to the experimental lifetimes of the lowest $\frac{5}{2}^+$ states [in fact, one of the most recent individual lifetime measurements of $\tau(^{29}\text{P } \frac{5}{2}^+) = 465 \pm 60$ (Ref. 48) gives $M_p = 18.5 \pm 1.2$ compared to $M_p = 21.0 \pm 1.2$ derived from the omnibus average lifetime from Table I and the theoretical values of 18.0 from Table V]. The systematic deviation of the $2 \rightarrow 0$ and $2' \rightarrow 0$ isovector transitions in $A = 26, 30$, and 34 is more indicative of a failure in the Chung-Wildenthal wave functions, since several of the lifetimes and branching ratios involved have been remeasured very recently.^{13,14,17,18} However, experimentally there is still the ambiguity in the relative signs of the $A = 34$ $2' \rightarrow 0$ transitions, as discussed in Sec. III D, and it is hoped that this can be resolved by hadron inelastic scattering experiments on ^{34}S which are sensitive to both neutron and proton components of the transition.

In most previous shell-model calculations for light nuclei the isovector effective charge has been "determined" or fixed to be close to free nucleon value, $e_p - e_n = 1$ (see, for example, Ref. 49). This is usually because harmonic-oscillator wave functions were used and/or because the matrix elements considered were predominantly isoscalar and hence were not sensitive to the isovector effective charge. In Ref. 30 the $E2$ transitions in nuclei with $A_c \pm 1$ and $A_c \pm 2$ around the closed shells $A_c = ^{16}\text{O}$ and ^{40}Ca were calculated with finite-well potentials. These potentials were effectively energy dependent since the potential depths for each orbit were constrained to reproduce the empirical separation energies (as given in Table 3 of Ref. 30). Hence, it is not surprising that the value of $e_p - e_n = 0.60$ obtained for $A = 18$ in Ref. 30 is essentially the same as the results from the present work with the

energy-dependent potential ($e_p - e_n = 0.58$). An important new result from the present study is that isovector transition strengths in all nuclei in the region $A = 16-40$ are consistent with this quenched isovector effective charge. Shell-model calculations for $A > 40$ are restricted to truncations even within the major oscillator shells, and hence, it is not particularly meaningful to compare the empirical effective charges needed for these calculations with our present results. However, it is interesting that some quenching of the isovector effective charge ($e_p - e_n \approx 0.8$) is deduced for transitions near ^{208}Pb ,⁵⁰ (The dependence of the effective charges on N and Z for heavy nuclei has been discussed in Refs. 51 and 53.)

The isoscalar effective charge is much easier to determine than is the isovector since most of the transitions in the sd shell are predominantly isoscalar and also there are many strong $T=0 \rightarrow 0$ transitions which are purely isoscalar. With harmonic-oscillator wave functions the isoscalar effective charge is quite state and mass independent and has a value $e_p + e_n = 1.70$. From a comparison of the theoretical quantities $A_p + A_n$ obtained with harmonic-oscillator and finite-well potentials in Table IV, we can see that the corresponding empirical values based on the finite-well potentials are about $e_p + e_n = 1.65(1.60)$ for the local (energy-dependent) potential.

The renormalizations of the effective charges from the free-nucleon values $e_p + e_n = 1$ and $e_p - e_n = 1$ ($e_p = 1$ and $e_n = 0$ in units of e), are related to the collectivities of the isoscalar and isovector quadrupole giant resonances, respectively.⁵¹⁻⁵⁴ In the random phase approximation (RPA) model with a schematic $Q \cdot Q$ particle-hole interaction, an attractive interaction lowers the collective particle-hole state from its unperturbed value and couples to valence particles coherently in the matrix elements of the operator Q . For a repulsive interaction the collective state is raised and couples incoherently. The polarizability χ is defined by

$$e_r^{\text{eff}} = e_r^{\text{bare}}(1 + \chi_r), \quad (38)$$

where $e_0^{\text{eff}} \equiv e_p + e_n$, $e_1^{\text{eff}} \equiv e_p - e_n$, and $e_0^{\text{bare}} = e_1^{\text{bare}} = e$. In the RPA approximation with a schematic interaction $Q \cdot Q$ the relation takes the simple form⁵²

$$\chi_r = (\epsilon/E_r)^2 - 1, \quad (39)$$

where ϵ is the unperturbed energy of the giant resonance which is approximately $2\hbar\omega$ for the quadrupole resonance and E is the perturbed energy rela-

tive to the ground state. (It has also been assumed that the energy difference between the model space states is much less than ϵ and it is easy to generalize when this is not the case.⁵¹) The original model of Mottelson⁵⁵ based on self-consistency gave $\chi_0 = 1$ and hence $E_0 = \sqrt{2}\hbar\omega$. Experimentally, the centroid of the giant isoscalar quadrupole resonance is fairly well established in heavy nuclei⁵⁶ at

$$E_0 = 65A^{-1/3} \text{ MeV} = (0.79)(2\hbar\omega)$$

(using $\hbar\omega = 41A^{-1/3}$ established from the proton rms radii of heavy nuclei) which gives $\chi_0 = 0.59$. This is the same as the isoscalar $E2$ polarization charge we required in the sd shell. Below mass 40 the isoscalar giant resonance is not experimentally so well established.^{56,57} The above comparison implies that $E_0 = (0.79)(2\hbar\omega)$ is also applicable to sd shell nuclei. As an example for ^{28}Si , using $\hbar\omega = 12.42$ MeV deduced from the ^{28}Si rms radius in the oscillator model,⁴ $E_0 = 19.6$ MeV. The centroid of the observed strength in alpha scattering on ^{28}Si is about 18.3 MeV,⁵⁷ which is in reasonable agreement given the problems inherent in separating background and multipolarity in these alpha inelastic scattering experiments.

The energy of the isovector $E2$ giant resonance has been more difficult to experimentally establish even in heavy nuclei. In some heavy nuclei, electron inelastic scattering strength in the region of $E \approx 130A^{-1/3}$ MeV $= 1.58(2\hbar\omega)$ has been attributed to the isovector giant quadrupole.⁵⁶ This gives $\chi_1 = -0.60$, which is larger than the value we have found in the sd shell $\chi_1(sd) = -0.3$ to -0.4 . The implication is that the isovector giant resonance is somewhat less collective in light nuclei, but there is no experimental information. It is interesting to compare this situation with that of the familiar isovector giant-dipole resonance. In heavy nuclei⁵⁶ E_1 (dipole) $\approx 78A^{-1/3}$ MeV $= 1.90(\hbar\omega)$, and hence, χ_1 (dipole) $= -0.72$ (using $\epsilon = \hbar\omega$). The resulting hindrance in the low-lying isovector $E1$ transitions is well established.⁵¹ Based on the experimental ratio E_1/ϵ the isovector resonance becomes less collective in light nuclei⁵⁶ and hence follows the same pattern suggested above from the isovector $E2$ effective charge in the sd shell.

The above comparisons are made transparent by the schematic $Q \cdot Q$ interaction assumption. Calculations based on more realistic interactions may give quantitatively different results (analogous to the differences between the δ , $Q \cdot Q + \delta$, and $Q \cdot Q$ models of Sec. V A). It is beyond the scope of this paper to

discuss all of these differences and we refer the reader to the literature (for example, Refs. 51 and 58). A general comment which can be made is that most "realistic" interactions have a short range and as discussed in Sec. IV A result in effective charges (polarizabilities) which are more state and mass dependent than required empirically. This problem may be associated with the difficulty in incorporating higher order corrections into the effective in-

teractions which is also manifest in the effective-mass problem discussed in Sec. V C.

ACKNOWLEDGMENTS

This report is based on work supported by the U. S. National Science Foundation, Grant PHY 80-17605 and by the U. S. Department of Energy, Contracts W-7405-ENG-48, DE-AC-02-76-ERO-3069, and EY-76-S-06-2227.

*Present address: Cyclotron Laboratory, Michigan State University, East Lansing, MI 48824.

†Permanent address: Department of Physics, Oregon State University, Corvallis, OR 97331.

¹B. A. Brown, W. Chung, and B. H. Wildenthal, *Phys. Rev. C* **21**, 2600 (1980); W. Chung, thesis, Michigan State University, 1976.

²E. K. Warburton and J. Weneser, *Isospin in Nuclear Physics*, edited by D. H. Wilkinson (North-Holland, Amsterdam, 1969), p. 173.

³A. M. Bernstein, V. R. Brown, and V. A. Madsen, *Phys. Rev. Lett.* **42**, 425 (1979).

⁴B. A. Brown, W. Chung, and B. H. Wildenthal, *Phys. Rev. C* **22**, 774 (1980).

⁵P. M. Endt, *At. Data Nucl. Data Tables* **23**, 3 (1979).

⁶P. M. Endt and C. Van der Leun, *Nucl. Phys.* **A310**, 1 (1977).

⁷A. Anttila, S. Brandenburg, J. Keinonen, and M. Bister, *Nucl. Phys.* **A334**, 205 (1980).

⁸E. K. Warbuton, J. W. Olness, and C. J. Lister, *Phys. Rev. C* **20**, 619 (1979).

⁹J. S. Forster, T. K. Alexander, G. C. Ball, W. G. Davies, I. V. Mitchell, and K. B. Winterborn, *Nucl. Phys.* **A313**, 397 (1979).

¹⁰J. J. A. Smit, M. A. Meyer, J. P. L. Reinecke, and D. Reitmann, *Nucl. Phys.* **A318**, 111 (1979).

¹¹R. Engmann, F. Brandolini, and I. Mauritzson, *Nucl. Phys.* **A171**, 418 (1971).

¹²E. K. Warburton, J. J. Kolata, and J. W. Olness, *Phys. Rev. C* **8**, 1385 (1973).

¹³K. Dybdal, J. S. Forster, P. Hornshoj, N. Rud, and C. A. Straede, *Nucl. Phys.* **A359**, 431 (1981).

¹⁴T. K. Alexander, G. C. Gill, J. S. Forster, W. G. Davies, I. V. Mitchell, and H.-B. Mak, *Bull. Am. Phys. Soc.* **26**, 1127 (1981).

¹⁵W. A. Sterrenburg and E. van Middelkoop, *Nucl. Phys.* **A291**, 269 (1977).

¹⁶D. E. L. Scherpenzeel, G. A. P. Engelbertink, H. J. M. Aarts, C. J. Van der Poel, and H. F. R. Arciszewski, *Nucl. Phys.* **A349**, 513 (1980).

¹⁷A. Anttila and J. Keinonen, *Phys. Rev. C* **21**, 1196 (1980).

¹⁸T. K. Alexander, G. C. Ball, J. S. Forster, W. G. Davies, I. V. Mitchell, and H.-B. Mak, *Bull. Am. Phys. Soc.* **26**, 537 (1981).

¹⁹A. R. Poletti, L. K. Fifield, J. Asher, and B. E. Cooke, *J. Phys. G* **5**, 575 (1979).

²⁰M. A. Meyer and J. J. A. Smit, *Nucl. Phys.* **A205**, 177 (1973).

²¹A. Anttila, M. Bister, and J. Keinonen, *Z. Phys. A* **274**, 227 (1975).

²²A. R. Poletti, A. D. W. Jones, J. A. Becker, R. E. McDonald, and R. W. Nightingale, *Phys. Rev.* **184**, 1130 (1969).

²³H. J. Maier, J. G. Pronko, and C. Rolfs, *Nucl. Phys.* **A146**, 99 (1970).

²⁴J. L. Durell, P. R. Alderson, D. C. Bailey, L. L. Green, M. W. Greene, A. N. James, and J. F. Sharpey-Schafer, *J. Phys. A* **5**, 302 (1972).

²⁵G. G. Frank, R. V. Elliott, R. H. Spear, and J. A. Kuehner, *Can. J. Phys.* **51**, 1155 (1973).

²⁶H. Grawe, K. Holzer, K. Kändler, and A. A. Pilt, *Nucl. Phys.* **A237**, 18 (1975).

²⁷P. J. Brussard and P. W. M. Glaudemans, *Shell Model Applications in Nuclear Spectroscopy* (North-Holland, Amsterdam, 1977).

²⁸M. Harvey and F. C. Khanna, *Nucl. Phys.* **A155**, 337 (1970); A. E. L. Dieperink and P. J. Brussard, *ibid.* **A129**, 33 (1969).

²⁹S. Fallieros and R. A. Ferrell, *Phys. Rev.* **116**, 660 (1959).

³⁰B. A. Brown, A. Arima, and J. B. McGory, *Nucl. Phys.* **A277**, 77 (1977).

³¹D. Vautherin and D. M. Brink, *Phys. Rev. C* **5**, 626 (1972).

³²M. Beiner, H. Flocard, N. Van Giai, and P. Quentin, *Nucl. Phys.* **A238**, 29, (1975).

³³C. B. Dover and N. Van Giai, *Nucl. Phys.* **A190**, 373 (1972).

³⁴J. W. Negele, *Phys. Rev. C* **9**, 1054 (1974).

³⁵G. E. Brown, J. S. Dehesa, and J. Speth, *Nucl. Phys.* **A330**, 290 (1970); V. Bernard and C. Mahaux, *Phys. Rev. C* **23**, 888 (1981); A. Lejeune, *Nucl. Phys.* **A339**, 317 (1980); R. Sartar and C. Mahaux, *Phys. Rev. C* **21**, 2613 (1980); G. F. Bertsch and T. T. S. Kuo, *Nucl. Phys.* **A112**, 204 (1968); G. E. Brown, J. H. Gunn, and P. Gould, *ibid.* **46**, 598 (1963).

³⁶M. Miska, B. Norum, M. W. Hynes, W. Bertozzi, S. Kowalski, F. N. Rad, C. P. Sargent, T. Sasanuma, and B. L. Berman, *Phys. Lett.* **83B**, 165 (1979).

- ³⁷C. G. Li, M. Y. Yearian, and I. Sick, *Phys. Rev. C* **9**, 1861 (1974).
- ³⁸I. Sick, private communication.
- ³⁹J. L. Durell, C. Harter, and W. R. Phillips, *Phys. Lett.* **70B**, 405 (1977); and W. R. Phillips, private communication.
- ⁴⁰B. A. Brown, S. E. Massen, and P. E. Hodgson, *J. Phys. G* **5**, 1655 (1979).
- ⁴¹H. Tyrén, S. Kullander, O. Sundberg, R. Ramachandran, P. Isacson, and T. Berggren, *Nucl. Phys.* **79**, 321 (1966); G. J. Wagner, in *The Proceedings of the Minerva Symposium on Physics Held at the Weizmann Institute of Science, 1973*, edited by U. Similansky, I. Talmi, and H. A. Weidenmüller (Springer, Berlin, 1973), p. 16 and references therein; J. Mougey, M. Bernheim, A. Bussiere, A. Gillebert, P. X. Ho, M. Priou, D. Royer, I. Sick, and G. J. Wagner, *Nucl. Phys.* **A262**, 461 (1976); K. Nakamura, S. Hiramatsu, T. Kamae, H. Muramatsu, N. Izutsu, and Y. Watase, *ibid.* **A271**, 221 (1976).
- ⁴²H. D. Wohlfahrt, E. B. Shera, M. Y. Hoehn, Y. Yamazaki, and R. M. Steffen, *Phys. Rev. C* **23**, 533 (1981).
- ⁴³I. Sick, J. B. Bellicard, J. M. Cavedon, B. Frois, M. Huet, P. Leconte, P. X. Ho, and S. Platchkev, *Phys. Lett.* **88B**, 245 (1979), and private communication.
- ⁴⁴J. L. Durell, C. A. Harter, J. N. Mo, and W. R. Phillips, *Nucl. Phys.* **A334**, 144 (1980).
- ⁴⁵B. A. Brown and S. E. Massen (unpublished).
- ⁴⁶B. S. Reehal and B. H. Wildenthal, *Part. Nucl.* **6**, 137 (1973).
- ⁴⁷A. P. Zuker, B. Buck, and J. B. McGrory, *Phys. Rev. Lett.* **21**, 39 (1968).
- ⁴⁸T. Byrski, F. A. Beck, P. Engelstein, M. Forterre, and A. Knipper, *Nucl. Phys.* **A223**, 125 (1974).
- ⁴⁹E. C. Halbert, J. B. McGrory, B. H. Wildenthal, and S. P. Pandya, *Advances in Nuclear Physics* (Plenum, New York, 1971), Vol. 4, p. 315; A. Arima, M. Sakakura, and T. Sebe, *Nucl. Phys.* **A170**, 273 (1971); S. Shlomo and R. Moreh, *ibid.* **A110**, 204 (1968).
- ⁵⁰G. Astner, L. Bergström, J. Blomqvist, B. Fant, and K. Wikström, *Nucl. Phys.* **A182**, 219 (1972).
- ⁵¹A. Bohr and B. R. Mottelson, *Nuclear Structure* (Benjamin, New York 1975), Vol. II.
- ⁵²I. S. Towner, B. Castel, and L. Zamick, *Nucl. Phys.* **A365**, 189 (1981).
- ⁵³V. R. Brown and V. A. Madsen, *Phys. Rev. C* **11**, 1298 (1975); **17**, 1943 (1978).
- ⁵⁴M. W. Kirson, *Nucl. Phys.* **A337**, 194 (1980).
- ⁵⁵B. R. Mottelson, *The Many Body Problem Les Houches Lectures* (Wiley, New York, 1958).
- ⁵⁶F. E. Bertrand, in *Proceedings of the International Conference on Nuclear Physics*, edited by R. M. Diamond and J. O. Rasmussen (North-Holland, New York, 1981), p. 129.
- ⁵⁷A. van der Woude, in *Giant Multipole Resonances*, edited by F. E. Bertrand (Harwood, New York, 1979), p. 65.
- ⁵⁸T. T. S. Kuo and E. Osnes, *Nucl. Phys.* **A205**, 1 (1973).